FABRICATION AND CHARACTERIZATION OF THERMOELECTRIC NANOLAYER THIN FILMS MODIFIED BY MeV Si IONS

by

MUHAMMED E GULDUREN

A THESIS

Submitted in partial fulfillment of the requirements

for the degree of Master of Science

in

The Department of Physics

to

The School of Graduate Studies

of

The University of Alabama in Huntsville

HUNTSVILLE, ALABAMA

2014

In presenting this thesis in partial fulfillment of the requirements for a master's degree from The University of Alabama in Huntsville, I agree that the Library of this University shall make it freely available for inspection. I further agree that permission for extensive copying for scholarly purposes may be granted by my advisor or, in his/her absence, by the Chair of the Department or the Dean of the School of Graduate Studies. It is also understood that due recognition shall be given to me and to The University of Alabama in Huntsville in any scholarly use which may be made of any material in this thesis.

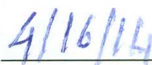

(Student signature) (Date)

THESIS APPROVAL FORM

Submitted by Muhammed E Gulduren in partial fulfillment of the requirements for the degree of Master of Science in Physics and accepted on behalf of the Faculty of the School of Graduate Studies by the thesis committee.

We, the undersigned members of the Graduate Faculty of The University of Alabama in Huntsville, certify that we have advised and/or supervised the candidate on the work described in this thesis. We further certify that we have reviewed the thesis manuscript and approve it in partial fulfillment of the requirements for the degree of Master of Science in Physics.

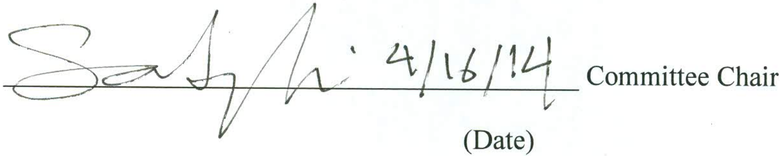
Committee Chair

(Date)

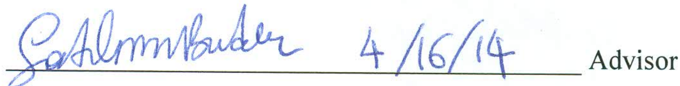
Advisor

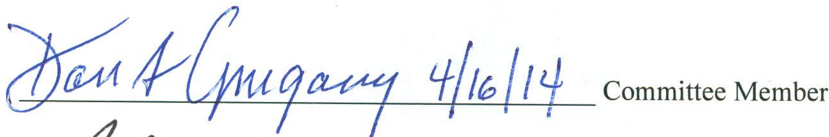
Committee Member

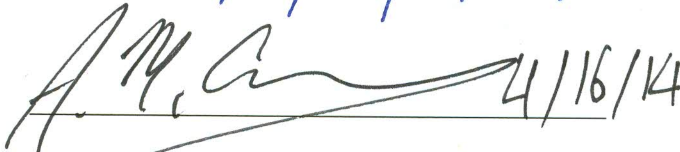

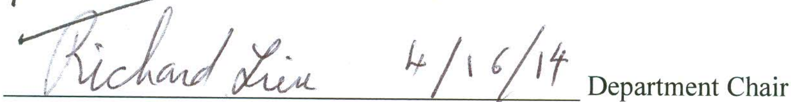
Department Chair

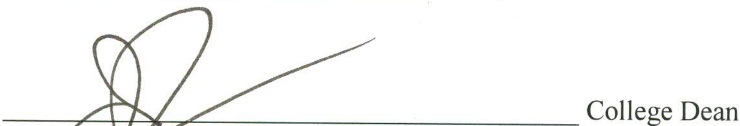
College Dean

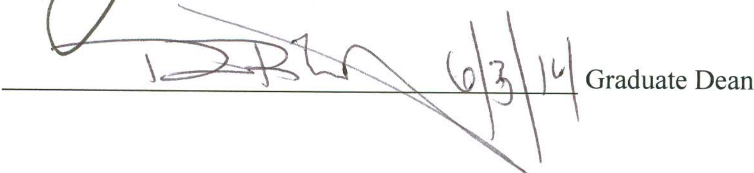
Graduate Dean

ABSTRACT

The School of Graduate Studies

The University of Alabama in Huntsville

Degree: Master of Science College/Dept. Science/Physics .

Name of Candidate: Muhammed E Gulduren .

Title: Fabrication and Characterization of Thermoelectric Nanolayer Thin Films Modified by MeV Si Ions.

Thermoelectric generators convert heat to electricity. A low thermal and a high electrical conductivity are characteristics of thermoelectric materials and devices. The efficiency of thermoelectric materials and devices is quantified by the dimensionless figure of merit

$$ZT = \frac{TS^2\sigma}{\kappa}$$

where S is the Seebeck coefficient, σ is the electrical conductivity, T is the absolute temperature in Kelvin, and κ is the thermal conductivity. Multilayer thin films with 100 alternating layers of SiO_2/SiO_2+Ge, 50 alternating layers of Si/Si+Sb, and 40 alternating layers of Si/Si+Ge superlattice thin films have been prepared using ion beam-assisted deposition (IBAD) and DC/RF sputtering in order to study thermoelectric power generation. Raman Spectroscopy, Atomic Force Microscopy for surface morphology, and annealing techniques were applied. The thermoelectric and transport features have been characterized for SiO_2/SiO_2+Ge, Si/Si+Sb, Si/Si+Ge superlattice thin films.

Abstract Approval: Committee Chair ______________________________

Department Chair ______________________________

Graduate Dean ______________________________

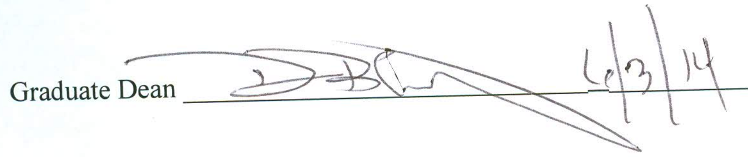

ACKNOWLEDGMENTS

The work described in this thesis would not have been possible without the assistance of a number of people who deserve special mention. First, I would like to thank Dr. Satilmis Budak for his dedicated guidance, assistance and patience. Secondly, I would like to thank my co-advisor Dr. Seyed Sadeghi for his time and assistance during this process and his help. The other members of my committee, Dr. Abdalla Elsamadicy and Dr. Don Gregory, have both been incredibly patient and helpful with comments and suggestions. Also, I would like to thank the Department of Electrical Engineering & Computer Science of the Alabama A&M University for giving me access to their facilities. Those who paved the way for my research have my utmost respect and without their diligence and expertise, my thesis would not have been possible. There are far too many to name but all of them are remarkable and highly intelligent individuals.

I would also like to thank my parents, Ismet and Sebahat Gulduren, to whom this thesis is dedicated. I cannot thank my parents enough for all the sacrifices they have made for me. They always consider my needs as a priority. Before passing every hurdle during my life journey, I depend on their priceless wisdom. Moreover, I also thank my parents for all the reasons I have faith in God. I would never have done it without their support, love and care. I love them with all my heart, pray for them and do my best to represent my family no matter where I am. I would also like to thank my siblings, Betul Ozunal and Omer Gulduren for the sincere relationship we have, and their support despite the long distance. I would also like to send my special thanks to Talat Ozunal for his support and for bringing more happiness to our family. He is a part of our family, and he is like a brother to me. I wish only the best for him.

TABLE OF CONTENTS

Page

List of Figures……………………………………………………………………….ix

List of Tables…………………………………………………………………………xii

Chapter

I. INTRODUCTION……………………………………………………….........1

1. Insulators, Conductors and Semiconductors ………………………………....2

A. Intrinsic Semiconductors…………………………………………….......5

B. Extrinsic Semiconductors…………………………………………….……..7

1. N-Type Semiconductors……………………………………….……..7

2. P-Type Semiconductors……………………………………….......10

2. Crystal and Atomic Structure of Semiconductors……………………......13

II. THERMOELECTRIC MATERIALS AND DEVICES………………………...19

A. Thermoelectric Materials………………..…………………………......19

B. The Thermoelectric Effect...………………………………………………...20

III. FABRICATION AND CHARACTERICATION TECHNIQUES……….…....23

A. Deposition Techniques………………………………………………..….23

1. Ion Beam Assisted Deposition (IBAD)……………………………....23

2. DC/RF Sputtering……………………………………………………….24

B. Characterization Techniques………………………………………………...25

1. Electrical Characterization…………………………………………....25

a. Van der Pauw sheet resistivity……………………………………....25

2. Thermoelectrical Characterization…………………………………….....26

a. Seebeck Coefficient Measurement………………………………..26

b. Thermal Conductivity Measurement Technique………………….....28

1. 3 ω Technique ………..……………………………………..28

3. Optical Characterization………………………………………........29

a. Atomic Force Microscopy Spectroscopy (AFM)…………………..29

b. Raman Spectroscopy……………………….............................30

4. Elemental Characterization Techniques……...……………….............31

a. Rutherford Backscattering Method (RBS)…………..……………......31

5. Modification of Thin Film Devices by Annealing and High Energy Beam Bombardment………..………………...………………………....33

a. High Energy Beam Modification for High Efficient Materials with AAMU Pelletron Accelerator……………………………………….33

b. Thermal Annealing…………………………………………….…....34

IV. EXPERIMENTAL METHOD……..………………………………...........36

V. RESULT AND DISCUSSION………………..……………………….......39

VI. CONCLUSION…………..…………………………………………….......54

APPENDIX A…...……..…………………………………………………...….56

APPENDIX B…...………………...………………………………………....…58

APPENDIX C...……………………………………………………………......….60

REFERENCES…….……………………………………...……………………....61

LIST OF FIGURES

Figure Page

1.1 Energy band gap diagram exhibiting energy band gap in (a) conductors, and (b) semiconductor, and (c) insulators……………………………………………………..3

1.2 Temperature dependence of the resistance in semiconductors…………………………...4

1.3 Temperature dependence of charge carrier concentration of intrinsic semiconductors…..6

1.4 Antimony atoms act as a donor in the simplified Ge lattice and create free electrons.......8

1.5 N-type semiconductors…………………………………………………………………8

1.6 Energy band gap for n-type semiconductor……………………………………………9

1.7 Temperature dependence of charge carrier concentration…………………………….…10

1.8 Acceptor impurity of boron creates a hole.………………………………………………11

1.9 P-Type Semiconductors……………………………………………………………...….11

1.10 Energy band diagram of p-type semiconductor………………………………………......12

1.11 Temperature dependence of charge carrier concentration……………………………….13

1.12 Unit cells……………………………………………………………………………….…...14

1.13 Crystal structure of Germanium (at T=0K)……………………………………………...15

1.14 Crystal structure of Ge atom at room temperature………………………………………15

1.15 Generation of electron hole pair in intrinsic semiconductor…………………….....….......16

1.16 Atomic structures of Si, Ge and Sb……………………………………………………...16

2.1 Thermoelectric effect.…....…………………………………………………….....…......21

3.1 Ion beam assisted deposition system...24

3.2 RF/DC Sputtering…………………….……………………………………….........25

3.3 Van der Pauw sheet resistivity set-up...……………………………………………......26

3.4 Seebeck effect………………………………………………………………..................27

3.5 Sample cross-section for thermal conductivity measurements……………………….......28

3.6 Atomic Force Microscopy set-up at CIM ………………...30

3.7 Olympus BX-40 Raman Spectroscopy set-up at CIM…………………………………...31

3.8 Rutherford Backscattering Spectrometry set-up at CIM……………………………......32

3.9 Pelletron 5 MeV Si Ion Bombardment set-up at CIM………………………………..34

3.10 Fisher Scientific Furnace set-up at CIM……………………………………………….35

4.1 Film geometry for Seebeck measurements…………..…………………………………..36

4.2 Modification of thin films by Si ion bombardment and heat treatment in the furnace…37

4.3 Quantum Dot formations on the superlattice multilayer thin films ……………………..38

5.1 Top view of the SiO_2/SiO_2+Ge thin films……………..39

5.2 The fluence dependence of the cross-plane Seebeck coefficients of SiO_2/SiO_2+Ge multilayer thin films (a) at the different temperatures (b) at room temperature…………………………………………………………………………....41

5.3 The fluence dependence of the cross-plane Seebeck coefficients of Si/Si+Sb multilayer thin films (a) at the different temperatures (b) at room temperature…..…41

5.4 The fluence dependence of Van der Pauw resistivity measurements of SiO_2/SiO_2+Ge multilayer thin films (a) at various temperatures (b) at 300 K…………..42

5.5 The fluence dependence of Van der Pauw resistivity measurements of Si/Si+Sb multilayer thin films at various annealing temperatures……………...…..….43

5.6 The fluence dependence of Van der Pauw resistivity measurements of Si/Si+Sb multilayer thin films at the room temperature…………………………..……..43

5.7 Raman Spectra of the thin films with 100 multilayers of SiO_2/SiO_2+Ge………………..45

5.8 (a) Details of Raman Spectra of Ge peaks (b) Raman Spectra of Si peaks (c) Raman spectra of $Si=O_2$ bonds…………………………………………………….46

5.9 (a) Raman Spectrum of unnanealed 50 multilayers of Si/Si+Sb thin films, (b) Raman Spectrum of 50 multilayers of Si/Si+Sb thin films annealed at 100 ^{0}C……..47

5.10 Atomic Force Microscopy AFM image of unannealed 40 Multilayer of

Si/Si+Ge thin films…………………………………...……………………………….....48

5.11 Atomic Force Microscopy AFM image of 40 multilayers of Si/Si+Ge thin films annealed at 100°C…………………..49

5.12 Atomic Force Microscopy (AFM) image of 40 multilayers of Si/Si+Ge thin films annealed at 200°C………………………………………………………………………..49

5.13 Atomic Force Microscopy (AFM) image of unannealed Si/Si+Sb thin films……….......51

5.14 Atomic Force Microscopy (AFM) image of Si/Si+Sb thin films annealed at 100°C…....51

5.15 Atomic Force Microscopy (AFM) image of 50 multilayers of Si/Si+Sb thin film annealed at 200 ^{o}C…………………………………………….....……………....52

5.16 RBS and RUMP Simulation of Si/Si+Ge thin films……………………………….....53

5.17 RBS and RUMP Simulation of Si/Si+Sb thin films……………………………………..53

A.1 Energy band formation in a crystal……………………………………………………56

B.1 Energy distribution of electrons in metals……………………………………………….58

B.2 Position of the Fermi Energy Level for intrinsic semiconductor at 0 K……………….....59

C.1 Schematic of a Van der Pauw measurement technique……………………………….....60

LIST OF TABLES

Table Page

1.1 Position of semiconductor elements in the Mendeleev table…………………………….......5

CHAPTER I

INTRODUCTION

Providing a sustainable supply of energy to the world's population will become a major societal problem for the 21st century as fossil fuel supplies decrease and world demand increases [1]. Recently, research in thermoelectricity is directed toward new improved materials for autonomous sources of electrical power for specialized medical, terrestrial and space applications [2]. Thermoelectric materials are semiconductors that function as "heat pumps" and as heat-to-electricity converters. Thermoelectric power generation allows for small size, high reliability, and quiet operation. Efficient thermoelectric-based heat-to-electricity converters, however require higher performance materials than are currently available [3].

In a typical thermoelectric device, a junction is formed from two different conducting materials, one containing positive charge carriers (holes) and the other negative charge carriers (electrons). When an electric current is passed in the appropriate direction through the junction, both types of charge carriers move away from the junction and convey heat away, thus cooling the junction. Similarly, a heat source at the junction causes carriers to flow away from the junction, making an electrical generator [4].

The conversion of heat to electricity by thermoelectric devices could play a key role in the future for energy production and utilization. However, in order to meet that need, more efficient thermoelectric materials are required that are suitable for high-temperature applications [9]. Recently ‘‘open structured’’ semiconducting compounds for thermoelectric applications have become very popular due to their characteristically low-thermal conductivities. The host atoms in

such materials build up weak bonds with interstitial atoms occupying ‘‘voids’’ in these structures leading to localized vibration modes. These localized modes resonantly scatter acoustic-mode, heat-carrying phonons. This concept has been studied in the Skutterudite material system where very low-thermal conductivities are possible when the voids are filled with Lanthanide ions [29].

The conversion efficiency of TE devices is related to the dimensionless figure of merit (ZT), defined as

$$ZT = \frac{TS^2\sigma}{\kappa} \quad (1.1)\ [22]$$

where S, σ, T, and κ are the Seebeck coefficient, electrical conductivity, absolute temperature in Kelvin, and thermal conductivity, respectively. High-performance TE materials require high S, high σ, and low κ coefficients [10].

1. Insulators, Conductors and Semiconductors

Band theory (see Appendix A) explains why a solid is an insulator, conductor, or a semiconductor. Energy bands are filled by the electrons depending on each atom’s proton number. Electrons tend to fill the lowest available energy bands. First the valence band is the band that is almost filled completely by electrons when the temperature is stable at 0 K. These electrons are the carriers of electricity when they gather enough energy to leave their energy band and go up to a higher energy level. The electrons occupy states up to the Fermi level (see Appendix B). Conduction occurs by driving electrons into the conduction band, which starts at the Fermi level. The Fermi level is usually found at the center between the valence and conduction bands [35], [36], [37].

Insulators: When the valence band is full, the solid is considered an insulator. These materials do not conduct electrical current because the outer electrons are tightly bound. In other

words, in order for a valence electron to become free and transition into the higher band, the electron must gain enough energy. However, in the case of insulators, the energy gap between the valence band and conduction band is too large. Forbidden energy gaps in an insulator are around 5 eV or more (Fig. 1.1 (d)). On the other hand, it is possible that an insulator may become conductive if either its temperature is raised very high or a high voltage is applied across the insulator [23], [28], [39].

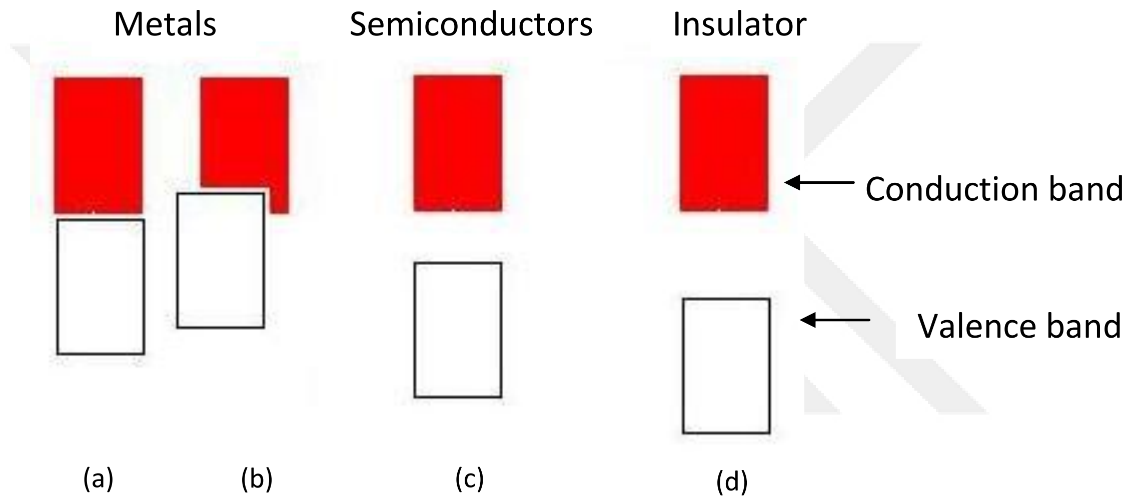

Figure 1.1 Energy band (see Appendix A) gap diagram exhibiting energy band gap in (a), (b) conductors, and (c) semiconductor, and (d) insulators.

Conductors: Band theory (see Appendix A and B) also explains the situation when materials show conductive behavior. There are two possible scenarios in this case. In the first case, the valence band is not completely filled. Electrons in the valence band can easily travel to the conduction band. However, the electrons will still need small amounts of energy to move between the conduction band and the valence band. (see Figure 1.1 (a)). In the second situation, there are some materials where the energy gap between the conduction band and valence band can be so small that they overlap (see Figure 1.1 (b)) [23], [40], [41].

Semiconductors: These are materials that show characteristics of both insulators and conductors. In semiconductors, the valence band is filled, and although they have an energy gap

between the valence band and the conduction band, the energy gap is not as large as in insulators, as shown in Figure 1.1 (c). The forbidden energy gap is about 1 eV (for example silicon, E_g= 1.12 eV and for Ge, E_g= 0.72 eV). Germanium and silicon are the best known semiconductors. It is even possible that at room temperature there might be transitions between the valence band and the conduction band. Semiconductors conduct electricity less than pure conductors and the resistivity of these materials is greater than that of a conductor. The conductivity depends on temperature and doping factors. The resistivity of semiconductors ranges from 10^{-4} to $10^{4}\Omega$m and it is possible to decrease it with an increase in temperature as seen in Figure 1.2. These materials are found with crystalline structures [23], [36], [39].

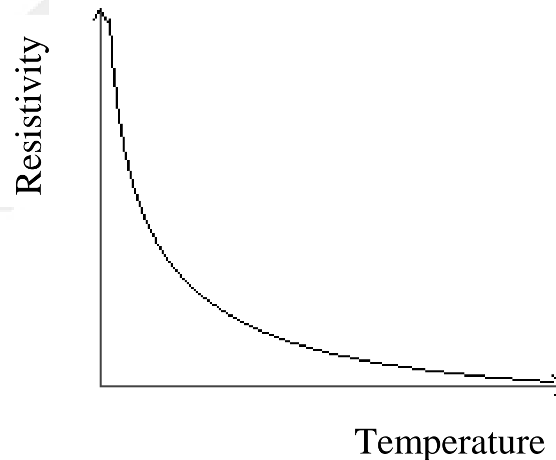

Figure 1.2 The temperature dependence of the resistivity in semiconductors [50].

Table 1.1 displays the semiconductors in Mendeleev's periodic table. There are two groups of semiconductors. The first one is elemental semiconductors found in group IV of the periodic table, and the second group contains the compound semiconductor materials that are the products of special combinations of group III and group V elements. In addition, impurity atoms can be added to semiconductors (indium, arsenic, gallium, etc.). Impurity atoms will give different electrical properties to the semiconductor [52].

Group → / ↓ Period	III	IV	V	VI	VII
II	B (Boron)	C (Carbon)			
III	Al (Aluminum)	Si (Silicon)	P (Phosphorus)	S (Sulfur)	
IV	Ga (Gallium)	Ge (Germanium)	As (Arsenic)	Se (Selenium)	
V	In (Indium)	Sn (Tin)	Sb (Antimony)	Te (Telluride)	I (Iodine)
VI					At (Astatine)

Table 1.1 Position of semiconductor elements in the Mendeleev table [53].

Semiconductors can be classified into two types: Intrinsic and extrinsic.

A. Intrinsic Semiconductors

An intrinsic semiconductor is the purest undoped form of semiconductor. A semiconductor can be classified as intrinsic if the impurity is less than 1 part in 100 million parts of semiconductor. As stated earlier, a semiconductor can become conductive when there is an increase in temperature. When the temperature rises, some electrons gain enough energy to make the transition from the top of the valence band to the lowest parts of the conduction band. Electrons convey charge through the semiconductor, so they are the called charge carriers or just carriers. After electrons make the transition, they leave holes in the valence band and these holes act like positive charges when a field is applied. The concentration of charge carriers varies, depending on the purity and the temperature of the semiconductor. Figure 1.3 illustrates the temperature dependence of the charge carrier concentration in an intrinsic semiconductor. The charge carrier concentration increases with temperature because more electrons make a transition from the valence band to the conduction band [23], [44].

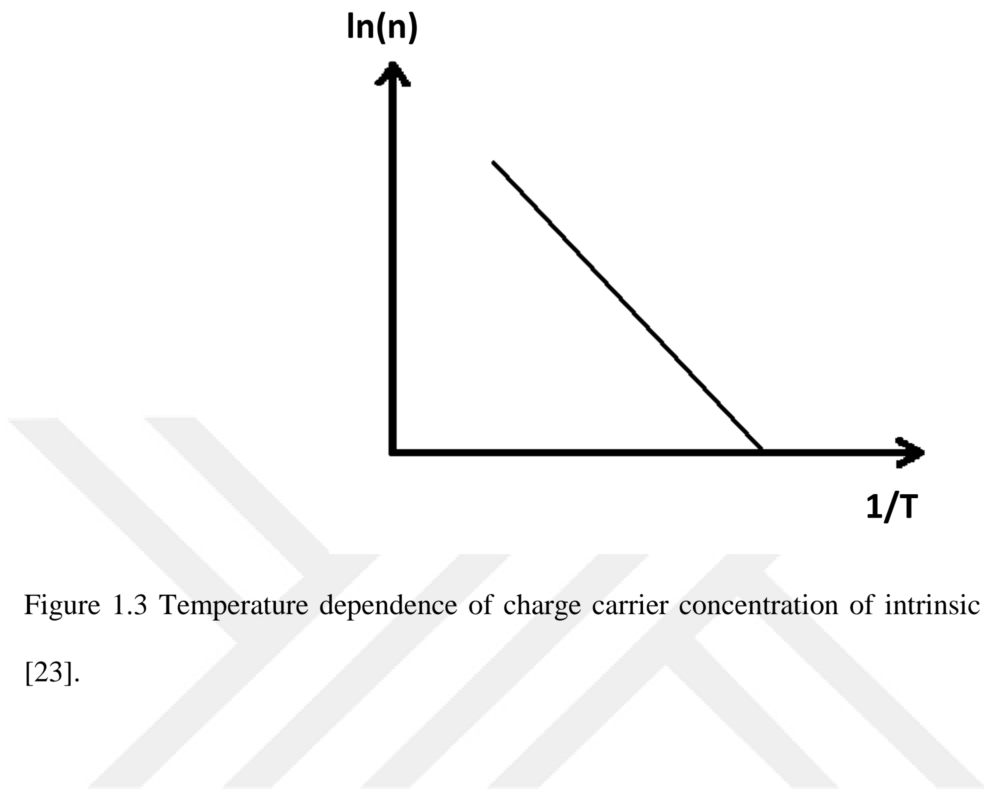

Figure 1.3 Temperature dependence of charge carrier concentration of intrinsic semiconductors [23].

B. Extrinsic Semiconductors

If an intrinsic semiconductor is doped with atoms that cause it to have different electrical properties, that semiconductor is called extrinsic. Doping atoms can be classified as either acceptor or donor depending on their effect on the intrinsic semiconductors. If the dopant material increases the hole concentration in the intrinsic semiconductor, it is called an acceptor impurity. On the other hand, if the impurity atoms donate extra valence electrons to the intrinsic atom's conduction band, it is called a donor impurity. Doping can be done by adding an appropriate number of impurity atoms. Therefore, the electrical conductivity can be changed considerably. Extrinsic semiconductors are divided into two groups [23], [36], [42]: N-type semiconductor and P-type semiconductor.

1. N-Type Semiconductors

If a pentavalent impurity that has 5 electrons in the outer shell (antimony (Sb), phosphorus (P), and arsenic (As)) is added to an intrinsic semiconductors like germanium or silicon, which have 4 electrons in their outer shell, those four electrons will form bonds with the semiconductor in the crystal and one electron will be left free in the crystal structure. As a result of this, n-type semiconductors are formed. Whit no change in the crystalline structure of the semiconductor, as shown in Figure 1.4 [23], [43].

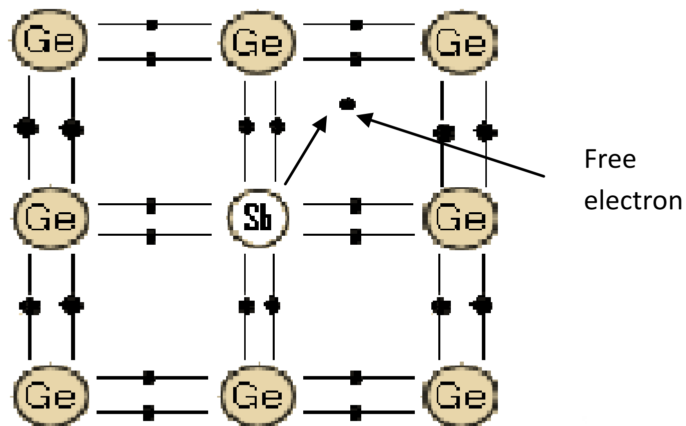

Figure 1.4 Antimony atoms act as a donor in the simplified Ge lattice and create free electrons.

As a result of this process, free electrons in the germanium crystal increase its conductivity considerably. In n-type semiconductors the majority of the charge carriers are the electrons whereas holes are minority carriers. The free electrons that are left by impurity atoms in the crystal can be seen in Figure 1.4 [23].

The semiconductor crystal doped by impurity atoms stays electrically neutral because free electrons and holes are formed in pairs. Figure 1.5 illustrates the free electron and hole concentration of the n-type semiconductor [23].

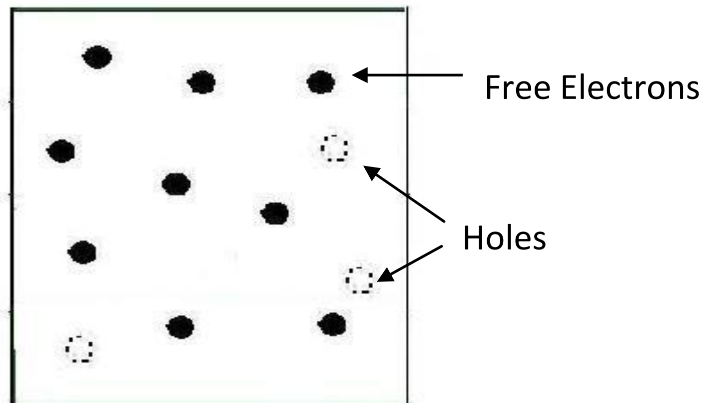

Figure 1.5 N-type semiconductors.

Energy bands (see Appendix A) in n-type semiconductors are different from those in intrinsic semiconductors as shown in Figure1.6. In n-type semiconductors other energy level exists. They are created by donor electrons and they are positioned close to the conduction band. This new energy band formation allows electrons to flow easier in n-type semiconductors [23], [36], [37].

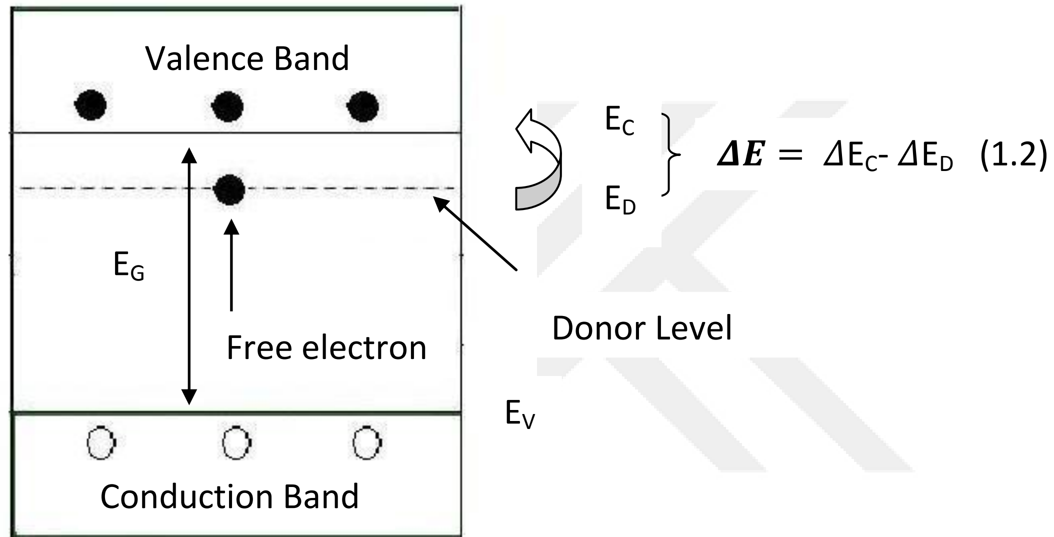

Figure 1.6 Energy band gap for n-type semiconductor.

Figure 1.7 shows the general temperature dependence of charge carrier concentration in n-type semiconductors. There is not a gradual increase in carrier concentration with temperature as the temperature rises from absolute zero. Donor electrons reach the conduction band quickly as the temperature increases. By the time the temperature reaches a certain quantity (T_D), there will be no more donor electrons left in the valence band. However, if the temperature keeps rising, there will be electrons making the transition from the valence band to the conduction band. At a temperature T_I , electrons from the valence band and electrons from the donor level are balanced. The extrinsic semiconductor will start to behave like an intrinsic semiconductor after this temperature [23], [36].

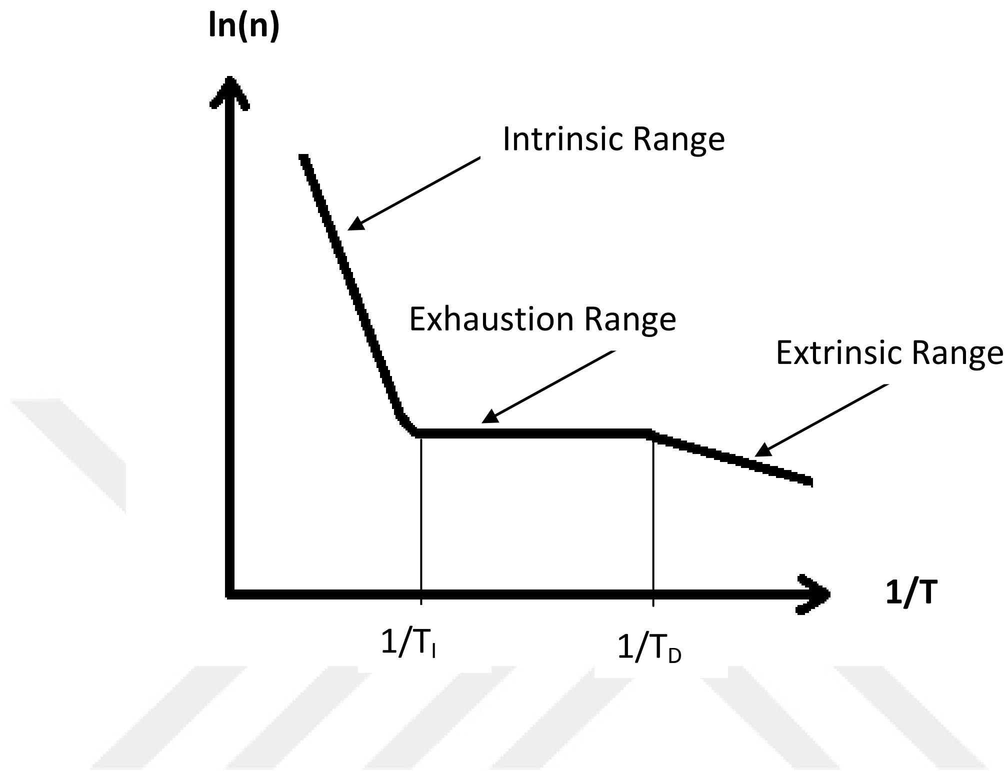

Figure 1.7 Temperature dependence of charge carrier concentration [53].

2. P-Type Semiconductors

If a trivalent impurity that has 3 electrons in the outer shell (gallium (Ga), indium (In), and boron (B)) are added to a pure semiconductor, the doping atoms will replace some of the semiconductor atoms in the crystalline structure as shown in Figure 1.8. These impurity atoms will leave a hole after they form only three covalent bonds. This trivalent impurity is known as an acceptor or p-type impurity. In this case, holes are the majority carriers of charge in the crystal as shown in Figure 1.9 [54].

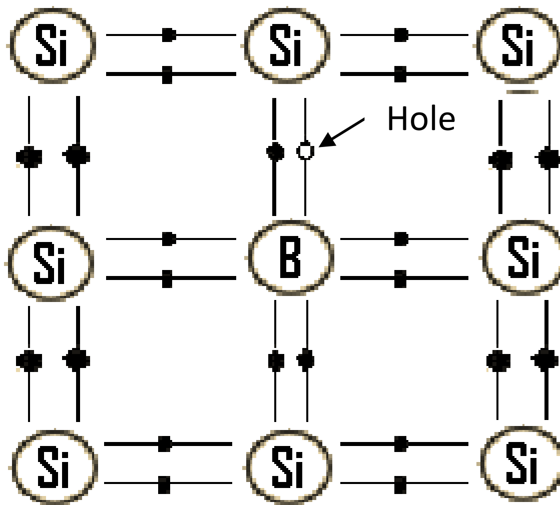

Figure 1.8 Acceptor impurity of boron creates a hole.

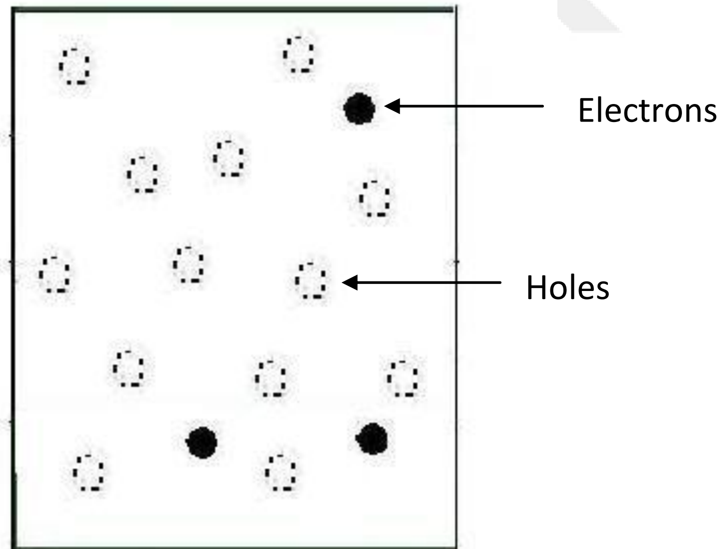

Figure 1.9 P-Type semiconductors.

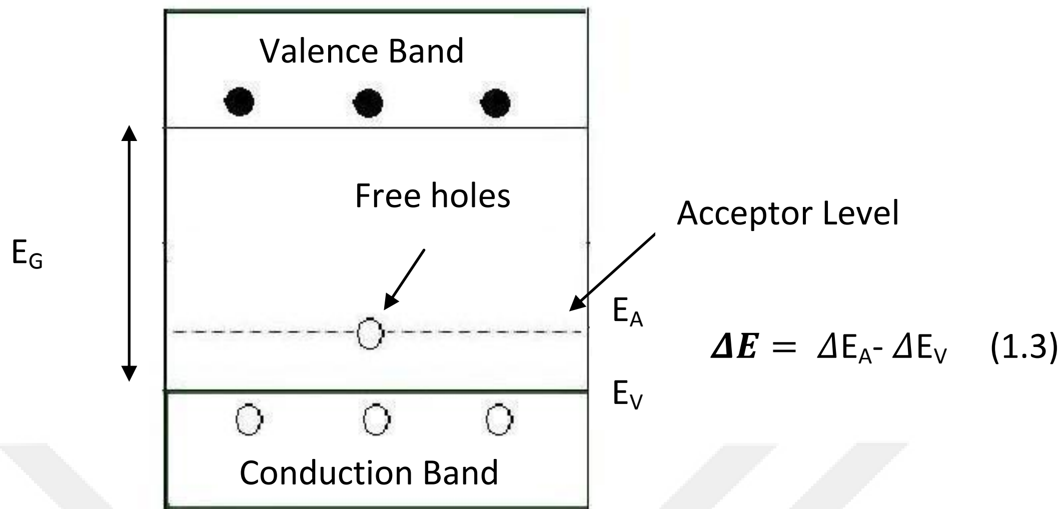

Figure 1.10 Energy band diagram of p-type semiconductor

At room temperature, after neighboring atoms migrate to complete the partial bonds, they will leave behind holes. This will cause a chain reaction and result in a current flow through the semiconductor. The newly created holes will help improve conductivity (see Figure1.10), but p-type semiconductors are not as conductive as n-type conductors. As a result of these holes, electrons in the valence band can be excited. In addition, due to the loss of electrons, the system is not neutral anymore. It has an excess positive charges [54].

Figure 1.11 shows the temperature dependence of charge carriers in p-type semiconductors. The behavior is similar to n-type semiconductors depending on the temperature. In this case, holes are the majority charge carriers. Also, another difference in n-type semiconductors is that they have an exhaustion phase between the extrinsic range and intrinsic range. In p-type semiconductors, this transition is called the saturation range [53], [54].

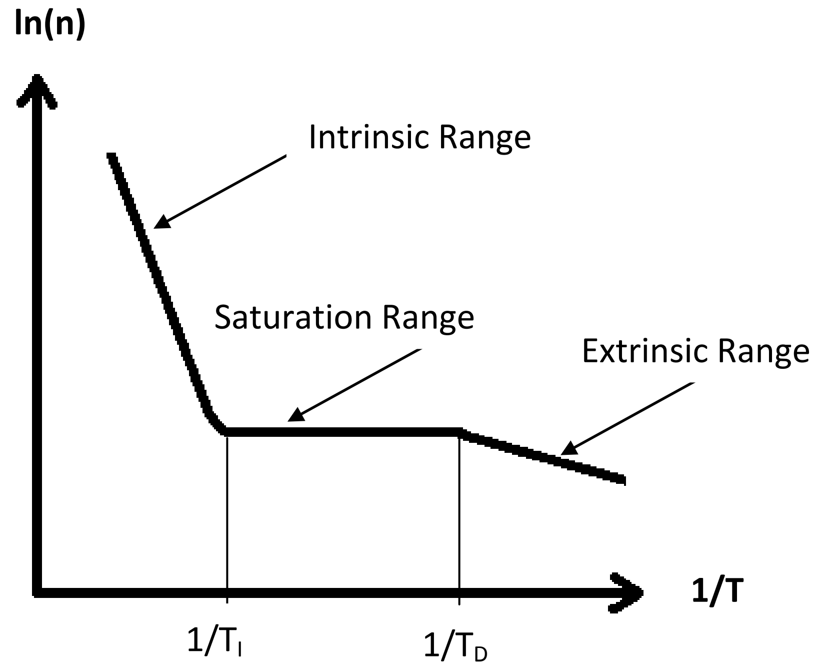

Figure 1.11 Temperature dependence of charge carrier concentration [53].

2. Crystal and Atomic Structure of Semiconductors

A crystal structure is a specific arrangement of atoms or molecules in a crystalline substance. Specifically, a crystalline structure has a 3-D order that repeats periodically and creates bonds with the nearest neighboring atoms. The crystal structure is composed of unit cells and lattices. A unit cell is a formation of one or more atoms arranged in three dimensions. Unit cells are the basics of the crystal structure and they specify the entire crystal structure according to the positions of the atoms within. Atoms take positions in a unit cell in four different ways; simple, side centered, body centered, and face centered as shown in Fig. 1.12 [45].

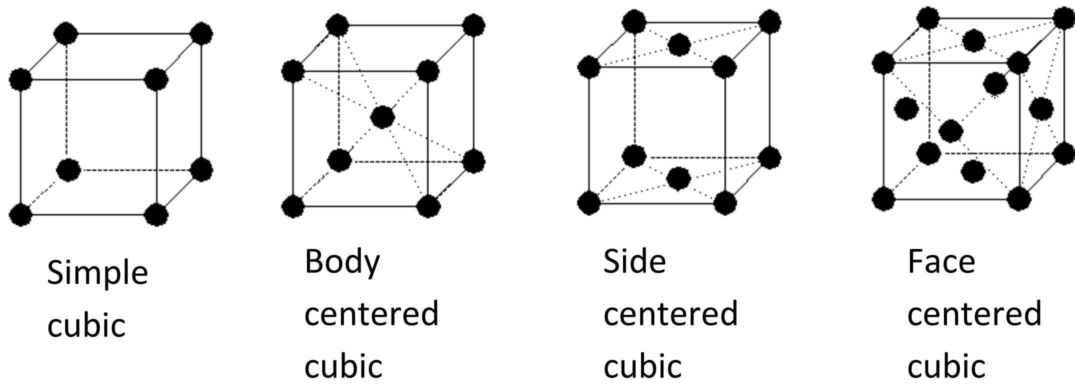

Figure 1.12 Cubic unit cells

Lattices are the geometric arrangement of points where atoms or molecules are positioned in a crystalline structure. That is, a single crystal of a crystalline material looks similar to all other crystals of that material. There are seven lattice systems: triclinic, monoclinic, orthorhombic, rhombohedral, tetragonal, hexagonal, and cubic [45].

Inside the crystal lattice there exists valence electrons in the outer shells. These electrons contribute to the formation of covalent bonds that keep the atoms together in specific structures in the lattice. Germanium (Ge) and silicon (Si) are the two most common semiconductors. A germanium atom has 32 electrons spread in four orbits while silicon has 14 electrons divided into three orbits. The outermost shell is called the valence orbit which contains 4 electrons in both cases, shown in Figure 1.13. The crystals are in a tetrahedral structure and each atom makes a covalent bond with one of its neighboring atoms [23], [45], [55].

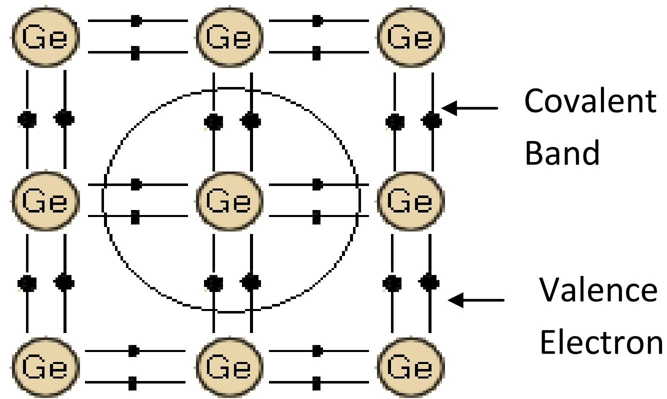

Figure 1.13 Crystal Structure of Germanium (at T=0K)

There will be no change in the crystal structure around absolute zero temperature. However, as temperature rises, the electrons that are bound tightly by covalent bonds will break away and become free from the crystal structure. Not only will there be free electrons in the system, but holes will also be formed (see Figure 1.14). Whenever a free electron occurs, a hole will be formed simultaneously. Thus free electrons and holes are always created in pairs when there is a positive temperature difference in the system. The motion between free electrons and holes increases the electric current in the direction of motion of the holes, shown in Figure 1.14. Free electron-hole pair generation is known as thermal generation in semiconductors, which can be seen in Figure 1.15 [23], [45].

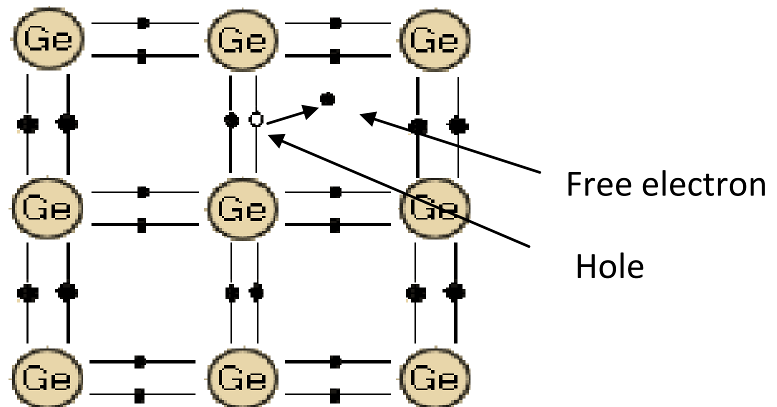

Figure 1.14 Crystal structure of Ge atom at room temperature

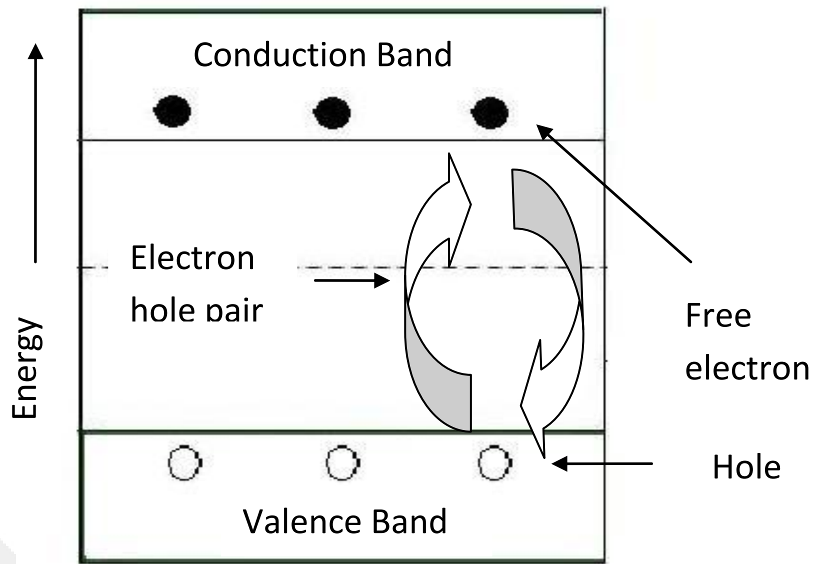

Figure 1.15 Generation of electron hole pair in an intrinsic semiconductor

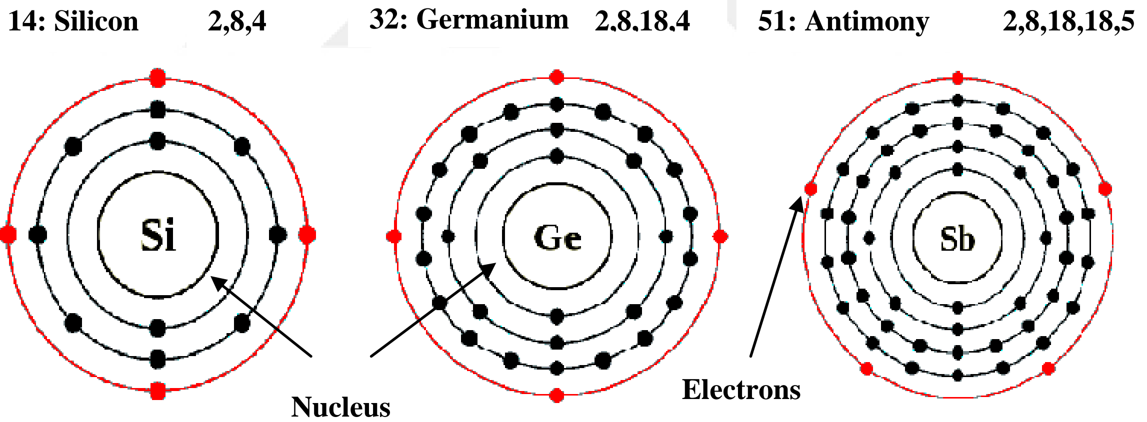

Figure 1.16 Atomic structures of Si, Ge and Sb

Figure 1.16 shows the structure of a silicon atom. It includes 14 protons and 14 neutrons in the nucleus. There are 14 electrons surrounding the nucleus in different orbits. The order of electrons in the shells are 2 electrons in the first shell, 8 electrons in the second shell, and 4 electrons in the outermost orbit. Furthermore, Figure 1.16 displays the atomic structure of a germanium atom. A germanium atom contains 32 protons and 32 neutrons. Besides the inner

electron shells, there are 4 electrons in the outer shell. The antimony atomic structure is also shown in Figure 1.16. It can be seen that the antimony atom has 51 protons and 51 neutrons. In the outermost shell are 5 electrons [56].

In general, the electrons in the inner orbits do not leave the atom. However, the electrons in the outermost shell are tightly bound to the nucleus. These electrons are known as free electrons. The other electrons in the inner orbits of the atom make tight bonds to the nucleus, and are called bound electrons. As mentioned previously, the free electrons in the valence shell may travel from one atom to another in the crystal lattice or they may travel among the atoms and make bonds with other neighboring atoms. Due to these free electrons in the material, electrical conduction occurs [46], [47].

There are a couple of theories that explain why atoms give or take electrons. The first approach is that chemical stability is a defining factor for atoms to give up their electrons. When an atom is chemically stable, it resists giving up electrons. However, if it is unstable, the electrons tend to be free. The level of stability is determined by the number of valence electrons, since the atom aims to completely fill its valence shell. If the electrons in the valence shell are more than half filled, then the atom tends to fill its shell. The maximum number of electrons that can be kept in the valence band is eight. Insulators have mostly five or more valence electrons and they try to gain electrons. Unlike insulators, conductors have four or fewer electrons in the outermost orbits and tend to empty their unfilled outer shells [40], [46].

Semiconductors, like silicon and germanium, have four valence electrons and are neither good conductors nor good insulators. On the other hand, the element antimony is considered an n-type impurity material. It has one more valence electron than semiconductors like silicon and germanium [57].

If atoms are described with respect to their energy bands, it can be said that an electron that is in the first shell possesses a small amount of energy. The greater the distance from the nucleus, the greater the total electron energy becomes [58].

If there is an external effect such as radiation, it can excite the electrons to the next energy level. However, those electrons that are excited to an upper energy state will not stay there. They will release the extra energy in the form of heat, light or other forms of radiation, and will return to their original energy levels [23].

CHAPTER II

THERMOELECTRIC MATERIALS AND DEVICES

A. Thermoelectric Materials

Thermoelectric (TE) materials are expected to be very important for high-temperature power generation applications, in particular, to store waste heat energy. The conversion of waste heat into electrical energy could take on an important role in the challenge to create a new energy technology which could lower the dependence on fossil fuels while decreasing greenhouse gas emissions [30].

Thermoelectric devices have no moving parts. Also they are silent, reliable, and scalable. However, in many applications, thermoelectrics have not been very cost effective. In the 1990s theoretical models showed that thermoelectric efficiency could be remarkably improved through nano-size engineering. This led to experimental studies in creating high-efficiency materials. Additionally, complex bulk materials (such as Skutterudites, Clathrates and Zintl phases) have been examined. It has been shown that achieving higher efficiencies is possible [31].

Materials that are considered as thermoelectrics usable in TE device applications include:

- Bismuth Chalcogenides
- Lead Telluride
- Inorganic Clathrates
- Magnesium group IV compounds
- Silicides
- Skutterudites

- Oxides
- Half-Heusler alloys
- Electrically conducting organic materials
- Silicon-germanium
- Functionally graded materials
- Nanomaterials [32]

B. The Thermoelectric Effect

The three best known thermoelectric effects are the Seebeck effect, the Peltier effect, and the Thomson effect. All basically explain the conversion of heat energy into electrical energy or vice versa [2].

As shown in Figure 2.1(a), the Peltier effect involves the conversion of an electric voltage into a temperature difference which can be used for refrigeration purposes. Applications include deep space processors, microprocessor cooling, automotive seat cooling, etc. Recently there have been many new findings in nanometer-scale structures, focusing on exploring thermoelectric properties [5]. The Peltier effect can be expressed mathematically as

$$j_Q = \Pi j \text{ x } (\kappa \Delta T) \quad (2.1)$$

Where:

• Π is the Peltier coefficient.

• j is the electric current density.

• κ – heat conductivity.

• j_Q – heat current density [75].

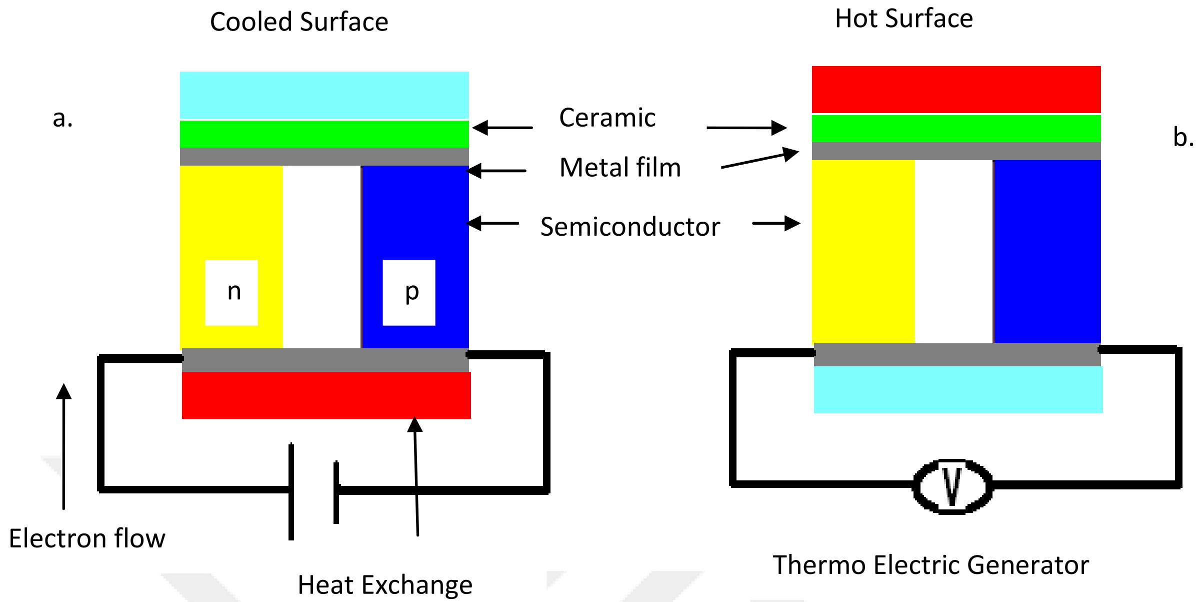

Figure 2.1 Thermoelectric effect.

As soon as a temperature gradient is introduced in a conductor, electrons are driven from the hot side to the cold side [7]. The electrical properties of the conductor define the path that the electrons will follow. In the case where electrons travel from the hot part toward the cooler part of the conductor, a negative thermoelectric emf (electromotive force) will be produced with respect to the hot end. Likewise, in a vice versa scenario, electrons go to the hot end from the cold end of the conductor; a positive thermoelectric emf is formed. This is known as the Seebeck effect, first recognized by physicist Thomas Johann Seebeck (1770-1831) [8]. This voltage, shown in Figure 2.1(b), known as the Seebeck emf, can be expressed as

$$E_{out} = \alpha\,(T_H - T_C) \qquad (2.2)$$

Where:

• $\alpha = dE / dT = \alpha_A - \alpha_B$

• α is the differential Seebeck coefficient or (thermo electric power coefficient) (volts/K) between the two.

α is positive when the direction of the electric current is in as the direction of the thermal current.

• E_{out} is the output voltage in volts.

• T_H and T_C are the hot and cold thermocouple temperatures, respectively, in K [8].

In 1854, Lord Kelvin (William Thomson) realized that if a temperature gradient is created in an electrical conductor, an energy interaction will be created in the system. This causes to form a power source that is either absorbed or rejected depending on the relative direction of the current and the temperature gradient. The power P' is proportional to the electric current I (A) and the temperature gradient $\frac{dT}{dx}$ (K/m), that is;

$$P' = \sigma(T) I \frac{dT}{dx} \quad (2.3)$$

where σ is the Thomson coefficient [59].

An active current flow will attract charge carriers to a region of different temperature. While charge carriers are being moved, they reject or absorb heat in order to remain in thermal equilibrium with their surroundings. However, there are reversible and irreversible effects in thermoelectricity. Due to the electrical resistivity of the conductors and the thermal contact, Joule heating occurs, which is an irreversible process. On the other hand, the thermal energy conveyed by the moving charges is reversible, which is known as the Thomson effect. In other words, the Thomson effect is the result of heat created by, or drawn from, the conductor depending on the product of the current density and the temperature gradient [6].

CHAPTER III

FABRICATION AND CHARACTERIZATION TECHNIQUES

A. DEPOSITION TECHNIQUES

1. Ion Beam Assisted Deposition

Ion beam assisted deposition (IBAD) is a thin film deposition technique that involves evaporation and concurrent ion beam bombardment in a high vacuum environment, as shown in Figure 2.1. The coating is formed by applying a high power electron beam first. After that, components are positioned into the vapor. Coating atoms or molecules condense and adhere to the surface of the substrate to produce the coating. Correspondingly, highly energetic ions (100-2000 eV) are produced and are directed onto the component surface. The substrate is placed at the intersection of the evaporator and ion beam. The concurrent ion bombardment distinguishes IBAD from any other thin film deposition technique. It noticeably enhances adhesion and it permits control over film features such as morphology, density, stress level, crystallinity, and chemical composition. Ion bombardment effectively combines the coating and substrate atoms. This prevents the columnar microstructure that is regularly observed in conventional, low temperature physical vapor deposition [33].

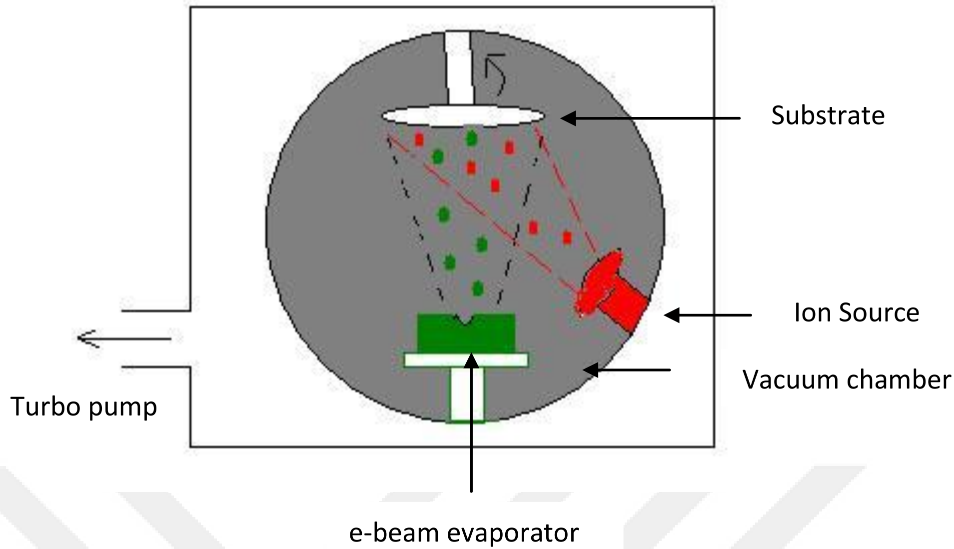

Figure 3.1 Ion beam assisted deposition system.

2. DC/RF Sputtering

DC or RF sputtering is chosen depending on the target material. If the target material is a conductor, a constant voltage will be ideal to accelerate the ions in order to have enough energy to extract sputtering atoms as they hit the target. Moreover, a conductor target will allow the resulting charges move freely and prevent any charge build up as the ions make contact with the surface. On the other hand, an insulator target will resist free charge movement in the material. If the ions which are accelerated by constant voltage are applied to the insulator target, charge will build up. As a result, the ion beam bombardment will not affect the surface anymore. An alternating current source is applied to the target so that the heavy ions will not follow the shifting, and only electrons will strike the target [49].

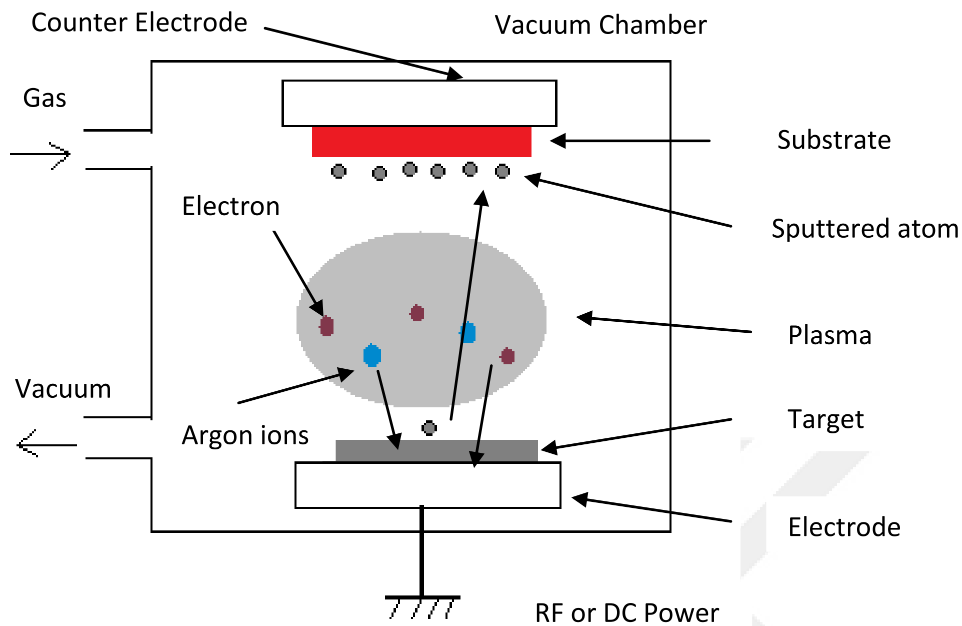

Figure 3.2 RF / DC Sputtering.

A. Characterization Techniques

1. Electrical Characterization

a. Van der Pauw sheet resistivity

The Van der Pauw sheet resistivity arrangement (see Appendix C) is used to measure the sheet resistivity of thin films and semiconductor wafers. The resistivity test helps determine the quality of thin films deposited on a silicon wafer. The sheet resistance is measured by sending a DC current through the outer two probes, while the stage is raised until slight contact has been made by the wafer and probe tips. In this way, an electrical circuit is formed. Thus, this circuit creates a voltage difference in the inner two probes and the resistivity values can be read through a digital multi-meter [24].

Figure 3.3 Van der Pauw sheet resistivity set-up.

2. Thermoelectrical Characterization

a. Seebeck Coefficient measurement

Seebeck coefficient measurements are important for examining semiconductors and metals for thermoelectric power generations applications. Thermoelectric power is a promising alternative energy source, to reduce the use of fossil oil in the future. The idea behind thermoelectric power generations is the conversion of heat to useful electric power. It can be applied in many areas, like the automobile industry, which consumes a large percentage of fossil sources today [47], [48].

The Seebeck effect is the physical principle of the thermocouple. In practice, a thermocouple is a thermoelectric device made of two different metals bonded at two points with a voltmeter positioned between two junctions, as shown in Figure 3.4. Since metals are conductors, the electrons are free to move. The electrons tend to travel from the hot junction to the cold. In the case where the wires are the same metal, the voltmeter shows no voltage difference because the electrons are distributed evenly. However, if the connected wires are made of different metals,

there will be a voltage difference between junctions. This result is caused by the difference in transport properties of the two metals. The free electrons belonging to the two different metals will also have a difference in their speeds. The Seebeck coefficient is defined as a thermoelectric measure of the magnitude of the voltage produced by a temperature gradient across a material [47], [48].

$$S = \frac{\Delta V}{\Delta T} \qquad (3.1)$$

In semiconductors, this affects the majority carriers (holes for p-type or electrons for n-type). The movement of carriers from a hotter area to a cooler one forms a dc potential. For electrons this creates a negative voltage and for holes this creates a positive voltage. Since there are many variables in the process of making semiconductor materials, such as doping densities and the crystallinity phase, it is not possible to calculate the Seebeck coefficient directly. Therefore, it must be measured experimentally [47], [48].

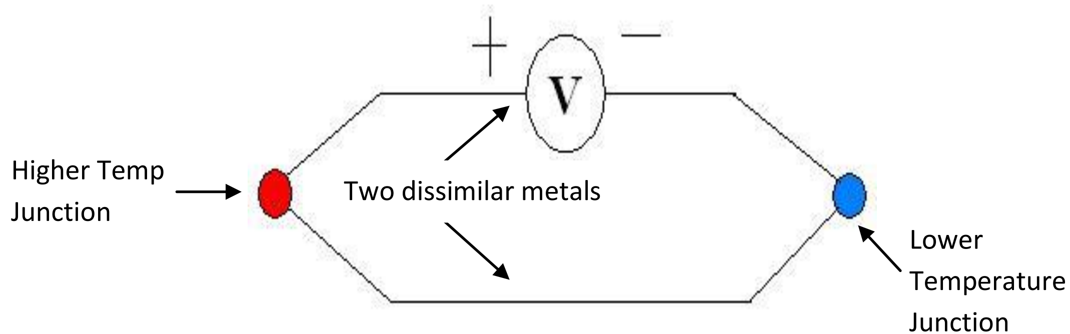

Figure 3.4 Seebeck effect.

b. Thermal Conductivity Measurement

1. 3 ω Technique

Figure 3.5 shows the geometry of the samples as a cross-section for the cross-plane 3ω thermal conductivity measurement. Thermal conductivity and heat transfer processes in superlattice structures are important in studies on low thermoelectric and thermionic devices [73].

In the 3ω technique, a micro-fabricated metal wire is placed on the specimen to act as an antenna and resistive heater. An alternating current (ac) voltage signal passes through the specimen to drive the heater with a frequency ω. At a frequency of 2ω, there are oscillations in the electrical resistance of the metal as a result of the periodic heating process. There is also a third harmonic (3ω) in the voltage signal, which determines the magnitude of the temperature oscillations. In conclusion, thermal properties of the specimen depend on the frequency of these oscillations [28].

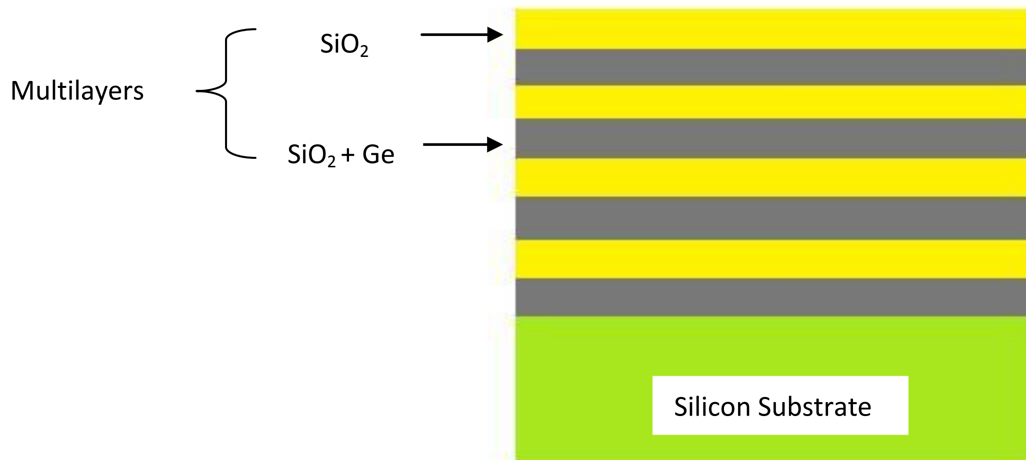

Figure 3.5 Sample cross-section for thermal conductivity meaurements.

3. Optical Characterization

a. Atomic force microscopy

Atomic force microscopy (AFM) is one of the many techniques of Scanned Probe Microscopy (SPM). The Scanning Tunneling Microscope (STM) was the first of many techniques of SPM and developed by Binnig & Rohrer, who were awarded the Nobel Prize for Physics in 1986. STM uses the tunneling of electrons (as a reference point) injected through a sharp metal probe tip in contact with the sample. However, AFM has been improved as an independent technique and has more application than SPM/STM. AFM examines surface morphology and properties by using a fine tip contacting the surface. AFM was invented by G. Binnig, C.F. Quate and Ch. Gerberin in 1985. A constant force is applied to the sample by the probe while the probe follows parallel lines scanning the sample across its surface. This establishes a three dimensional map of the sample as the probe analyzes the surface. The motion of the probe over the surface is controlled by piezoelectric translators in the X and Y directions.

AFM capabilities;

- Applicable in air or water,
- Creates a topographic map on the nanometer-scale,
- Usable on surfaces that are not good conductors,
- Can also measure mechanical, magnetic, electric, optical, thermal, and chemical properties [18].

Figure 3.6 Atomic Force Microscopy set-up at CIM.

b. Raman Spectroscopy

Raman spectroscopy was first developed in 1927. Since then, it has been very attractive not only for material research but also for spectroscopic measurements. Lasers with monochromatic photons at high flux densities were essential in the history of Raman spectroscopy, and these developments have lead to substantial improvements in scattering signal amplitudes [19].

Raman spectroscopy employs the inelastic scattering characteristic of light. Firstly, an electron is transferred to the conduction band from its valence energy band by absorbing a photon. Then the excited electron in the conduction band emits (and/or absorbs) phonons. Finally, the electron returns to its original state emitting a photon. A Raman signal occurs when the photon, whose energy is smaller than that of the incident photon, is scattered. As a result, phonon frequencies will be created depending on the intensity and frequency [20].

Figure 3.7 Olympus BX-40 Raman Spectroscopy set-up at CIM.

4. Elemental Characterization Techniques

a. Rutherford Backscattering Spectrometry

In the surface layer analysis of solids, Rutherford Backscattering Spectrometry (RBS) has been the preferred method over the years. The method starts with bombarding a target with ions between 0.5–4 MeV. Then, it continues with energy measurements of the backscatter using a solid state detector. RBS analyzes the concentration of a material quantitatively and investigates individual elements for their thickness on samples as well. However, when it comes to examining light elements, RBS is not sensitive enough to detect the structures and other nuclear based methods, such as the nuclear reaction analysis (NRA) or the elastic recoil detection analysis (ERDA) must be used [17].

RBS measurements have been taken and analyzed by a computer program called Rutherford Universal Manipulation Program. It was first introduced by M. Thompson in 1985. This program determines the elemental compositions from the experimental spectrum. The program sees the structure as layers of the same concentration, thus requires real parameters for the concentrations and thicknesses of the layers. The RUMP code creates a hypothetical spectrum measurement and a depth profile analysis for targets with different thicknesses [24].

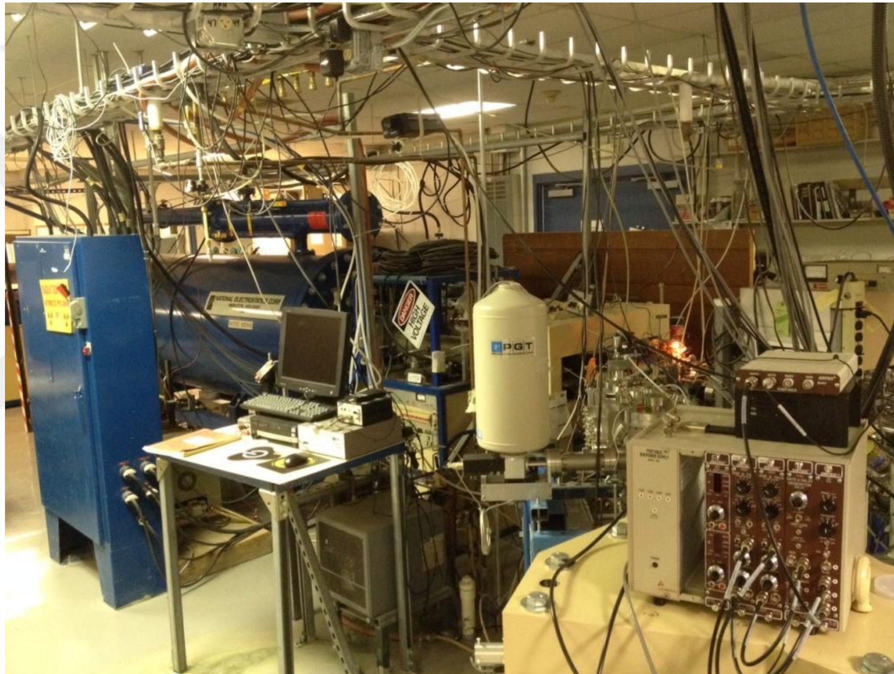

Figure 3.8 Rutherford Backscattering Spectrometry set-up at CIM.

5. Modification of Thin Film Devices by Annealing and High Energy Beam Bombardment

a. High Energy Beam Modification for High Efficient Materials with AAMU Accelerator

Defects in samples have been created using techniques such as metallic ion implantation and thermal annealing for years now in order to modify the linear and the nonlinear optical properties near the surface of silica glass. However, high energy beam bombardment seems to be more preferable over other defect creators for producing nano clusters [72].

The goal of this thesis research is to see if there is a change in the figure of merit values after bombarding the superlattice structure with MeV Si ions. The bombardment creates nanoscale quantum dot structures. An increase of the Seebeck coefficient and electrical conductivity is expected due to these structures. This is caused by an increase in the electronic density of states in the nano scale formations. Besides forming nano clusters, the bombardment will affect the whole structure of the samples, creating reflections at the lattice interfaces and the grain boundaries of these quantum dots formed by bombardment. In addition, the bombardment will increase the scattering of phonons, the inelastic collisions of phonons, and obstruct heat transport in a direction perpendicular to the lattice. Phonons are chiefly absorbed and then dissipated along the lattice, so the cross-plane thermal conductivity decreases [71].

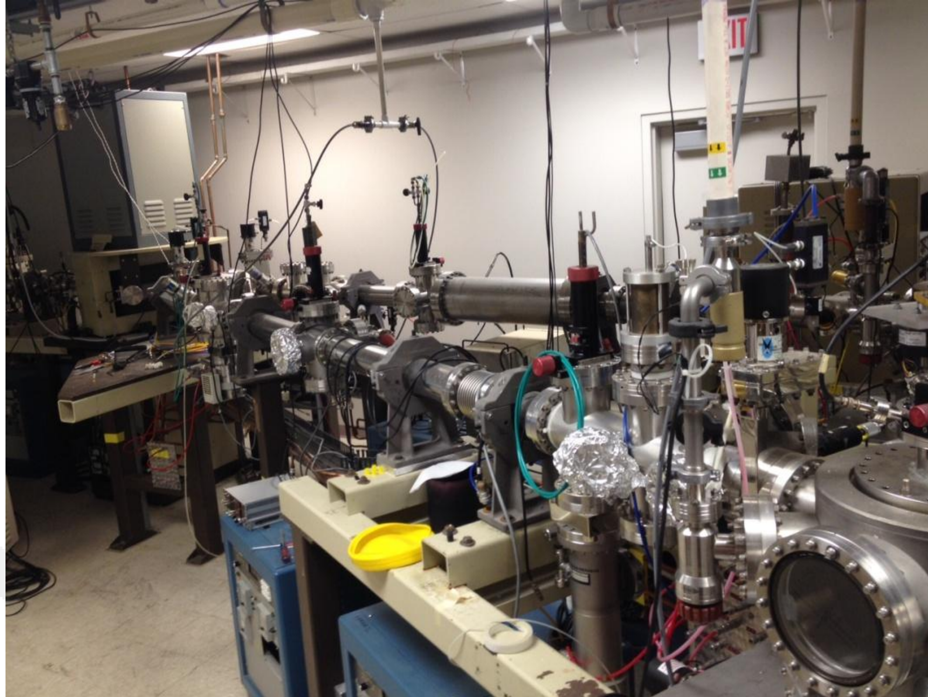

Figure 3.9 Pelletron 5 MeV Si Ion Bombardment set-up at CIM.

b. Thermal Annealing

Annealing can improve the microstructural and mechanical properties of materials. Annealing is a very well-known procedure which has been employed since ancient times. Metallurgists have heated materials, like metals in fire for long periods of time and then cooled them by burying or covering with clay or sand. Cycles of heating and cooling change the properties of materials with the goal of obtaining an improved structure. This process has undergone much advancement and can be accomplished accurately and neatly using a well controlled annealing furnace. This process has been used extensively in material science and in thin film physics research [34].

Annealing causes considerable changes in the structural, electrical and optical properties of semiconductor thin films. It can be used for many purposes such as mixing the elements in the

thin films to forming homogeneous structures, and promoting the inter-diffusion of multilayer thin films, thereby forming new materials with better thermal stability and lower resistivity. In addition, quantum dots can also be formed using thermal annealing techniques [62], [63].

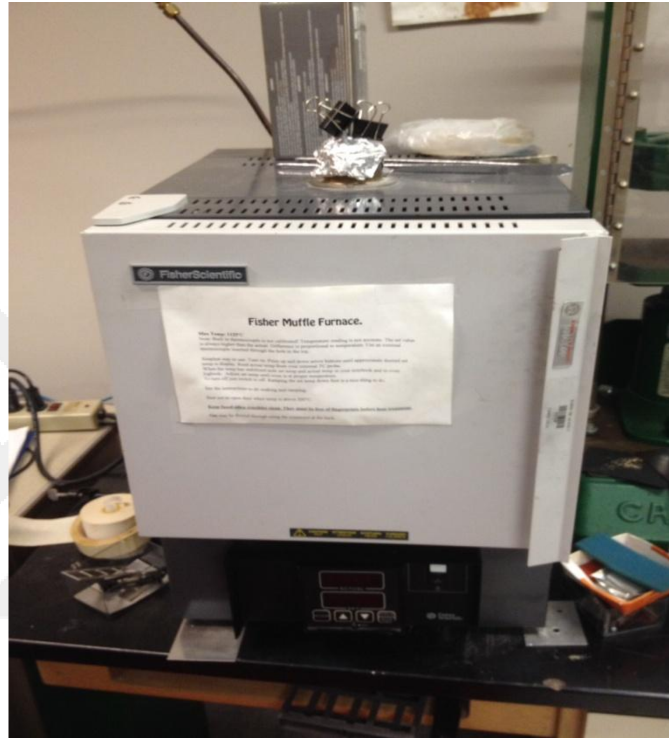

Figure 3.10 Fisher Scientific Furnace set-up at CIM.

CHAPTER IV

EXPERIMENTAL METHOD

Using ion beam assisted deposition (IBAD) and DC/RF Sputtering,100 alternating layers of SiO_2/SiO_2+Ge, 50 alternating layers of Si/Si+Sb, and 40 alternating layers of Si/Si+Ge nanolayers thin films have been deposited on silicon (Si) and fused silica (suprasil) substrates. The multilayers were formed by sequentially depositing SiO_2 and SiO_2+Ge, Si and Si+Sb, Si and Si+Ge layers on the substrates. These thin films build a periodic quantum well formation which includes 100 alternating layers with a total thickness of 134 nm of SiO_2/SiO_2+Ge, 50 alternating layers with a total thickness of 334 nm of Si/Si+Sb, and 40 alternating layers with a total thickness of 640 nm of Si/Si+Ge.

Two electron-gun systems have been used in both IBAD and DC/RF sputtering to evaporate two solids, turning each system on and off alternately, to form multilayers. The base pressure measured in the IBAD chamber was 5.3×10^{-6} Torr during the deposition process and 3×10^{-6} Torr in the DC/RF Sputtering chamber. The film geometries used for deposition and Seebeck measurements on SiO_2/SiO_2+Ge nano layers thin films are shown in Figure 4.1.

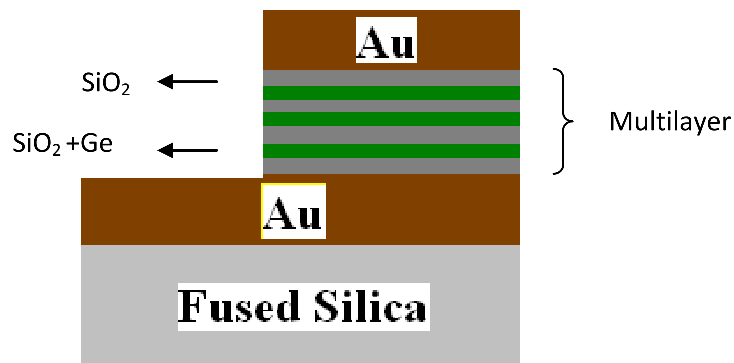

Figure 4.1 Film geometry for Seebeck measurements.

To form nano structures, as seen in Figure 4.2 and Figure 4.3 (nano dots and/or nano clusters), and defects in the thin films, two techniques have been used. One of the techniques is thermal annealing, and the other is high energy ion beam bombardment. The thermal annealing technique was applied to thin films for an hour at various temperatures. 5 MeV Si ion bombardment using the Pelletron ion beam accelerator at the Alabama A&M University Center for Irradiation of Materials (CIM) was also been used on these thin films. The thin films were bombarded using five different fluencies which were between 1×10^{12} ions/cm^2 and 7×10^{13} ions/cm^2. Before and after the annealing, the Dilor-JOBIN YVON-SPEX Raman Spectrometer was used to analyze the multilayer films for determining the order of the system and the bonds among the introduced elements in the multilayers. Also, surface morphologies of the thin films were obtained in this study with the AFM before and after the annealing. Finally, Rutherford Backscattering Spectrometry (RBS) was used to determine the total film thickness and stoichiometry of the multilayer super lattice thin films.

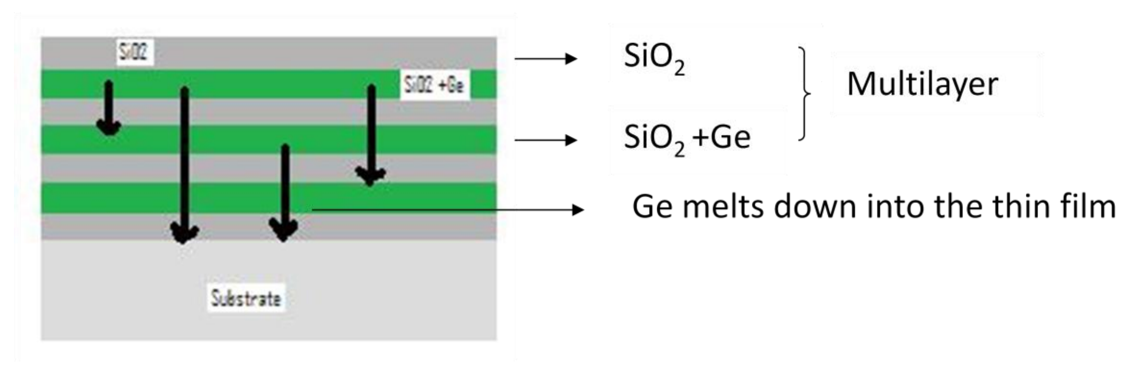

Figure 4.2 Modification of thin films by Si ion bombardment and heat treatment in the furnace.

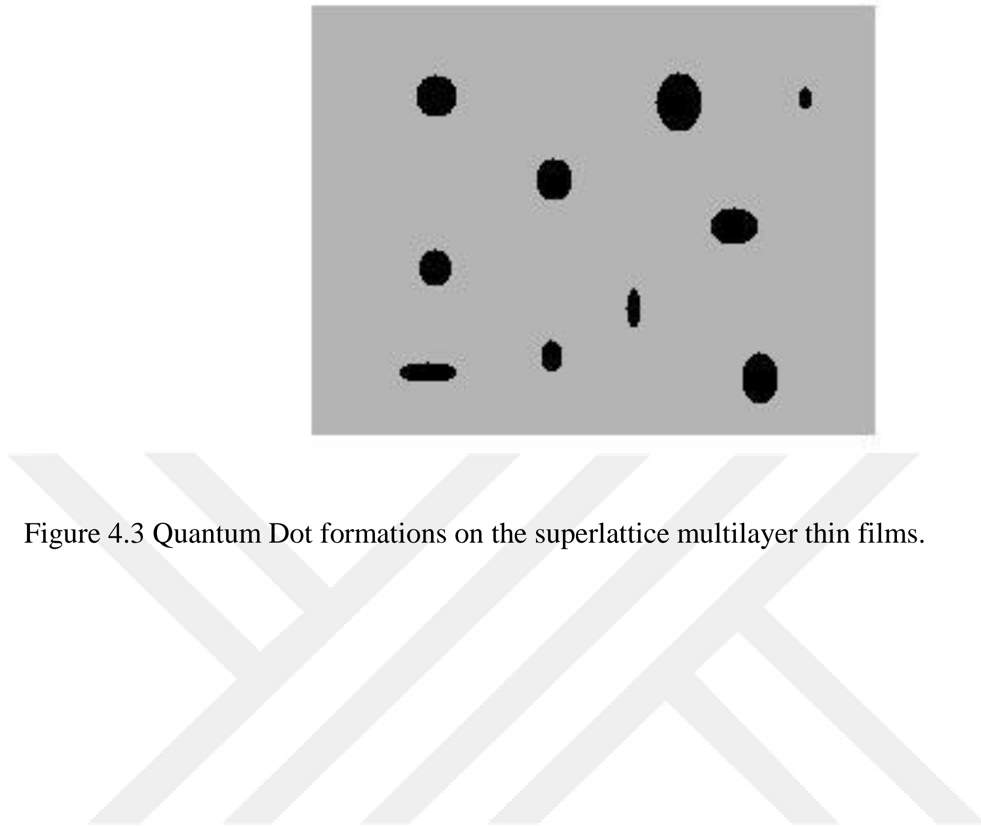

Figure 4.3 Quantum Dot formations on the superlattice multilayer thin films.

CHAPTER V

RESULTS AND DISCUSSIONS

Lately, there has been interest in Semiconductor devices because of their thermoelectric applications in cooling and power generation. Thermoelectric properties of semiconductors may vary depending on the orientation of the semiconductors. There were two orientations used while doing experiments on the thin films. The first was in-plane which was along the film plane, and the other was across-plane which was perpendicular to the film area. It is thought that a strong scattering interface may affect electrons and phonons in the cross-plane direction of thin films more than those in the in-plane direction. To understand thermoelectric power generation in the cross-plane direction, one needs to measure the Seebeck coefficient. This method has been applied to SiO_2/SiO_2+Ge thin films.

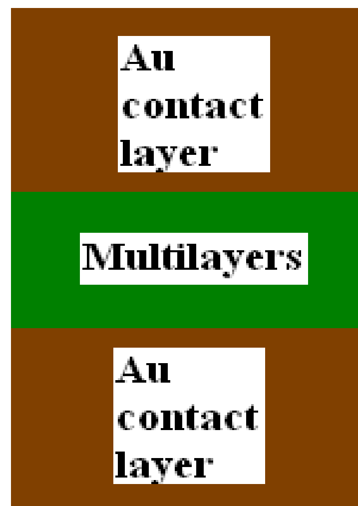

Figure 5.1 Top view of the SiO_2/SiO_2+Ge thin films.

The structure in Figure 5.1, was used to study the Seebeck coefficient. Since the Seebeck

coefficient of the Au lead is small compared to the semiconductor, the contribution of the lead is neglected in the experiment. Seebeck coefficients of SiO_2/SiO_2+Ge and Si/Si+Sb multilayer thin films at different fluencies are shown in Figure 5.2 and Figure 5.3. The original Seebeck values are negative, meaning there is negative thermo power, with electrons as the main charge carriers, in these structures. The cross-plane Seebeck coefficients in Figure 5.2 (a) display the fluence dependence at various temperatures. There is no obvious correlation. In Figure 5.2 (b), the temperature remained stable at 25 ^{0}C while the fluences were varied. The unbombarded sample's Seebeck coefficient is -175.33 μV/ K at 300 K as shown in Figure 5.2 (a). However, this value decreased to -344.02 μV/ K at 380 K as shown in Figure 5.2 (a). In Figure 5.2 (b), the maximum change in the Seebeck coefficient is at 300 K for fluencies of 1×10^{12} to $7x10^{12}$ (Si ions) ions/cm^2.

Figure 5.3 (a) illustrates the fluence dependence of the cross-plane Seebeck coefficient for 50 alternating layers of Si/Si+Sb thin films at different temperatures. The coefficient exhibited no clear trend with temperature or with fluence. A large Seebeck coefficient is one of the desired features of thermoelectric devices and thermoelectric materials. The largest Seebeck coefficient was measured for a fluence of $7x10^{12}$ ions/cm^2 at 300 K. An increase of the Seebeck values can be interpreted as an increase in the electron state density in the energy bands of the quantum dot formations created by ion bombardment [16], [61].

Each data point in Figures 5.2-5.6 represents an average of three measurements on the same sample. Error bars indicate the standard deviation. An investigation onto the physics that might explain some of the odd behavior shown in the figures is beyond the scope of this thesis. Because all standard deviations are about equal, error bars are not shown on all data points.

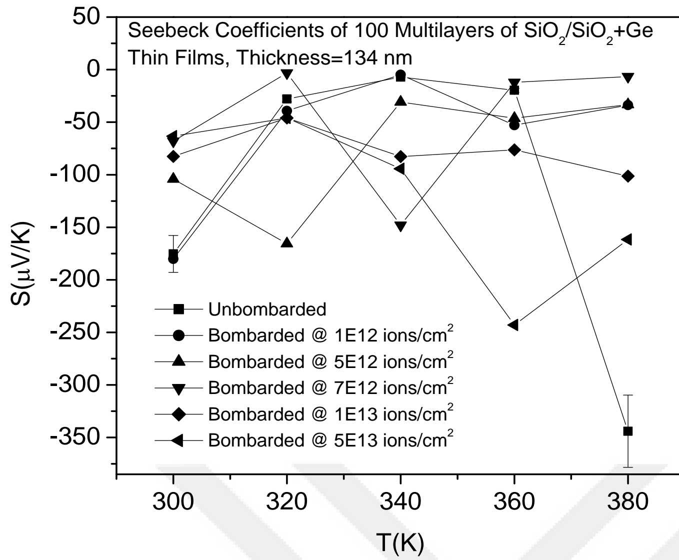

(a)

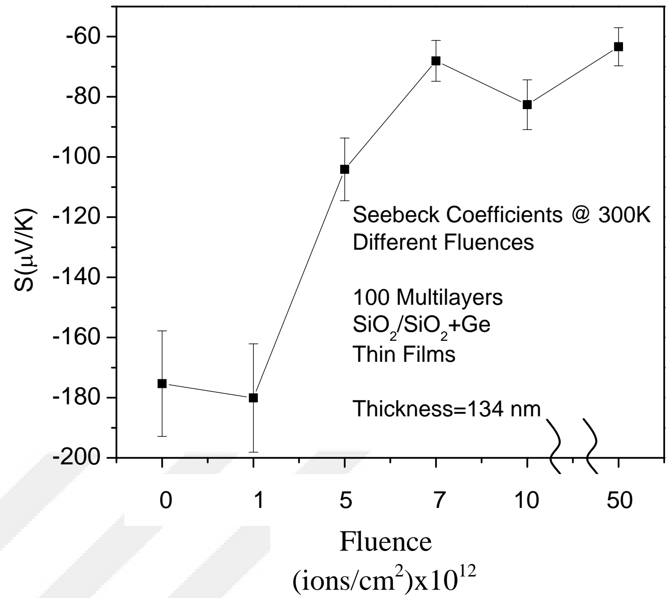

(b)

Figure 5.2 The fluence dependence of the cross-plane Seebeck coefficients of SiO_2/SiO_2+Ge multilayer thin films (a) at different temperatures (b) at room temperature.

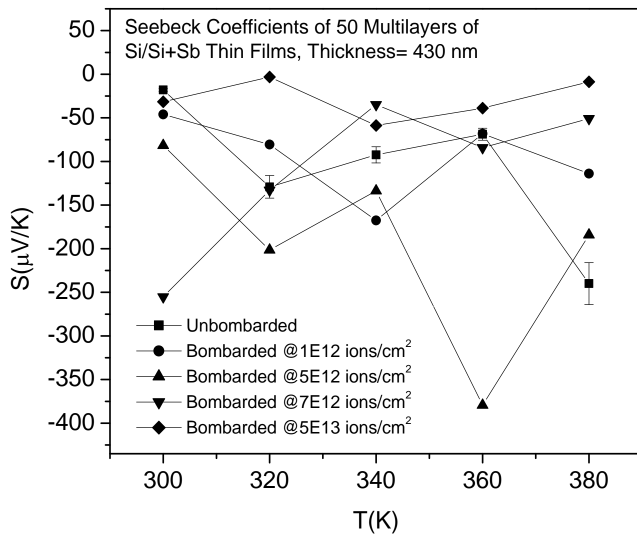

(a)

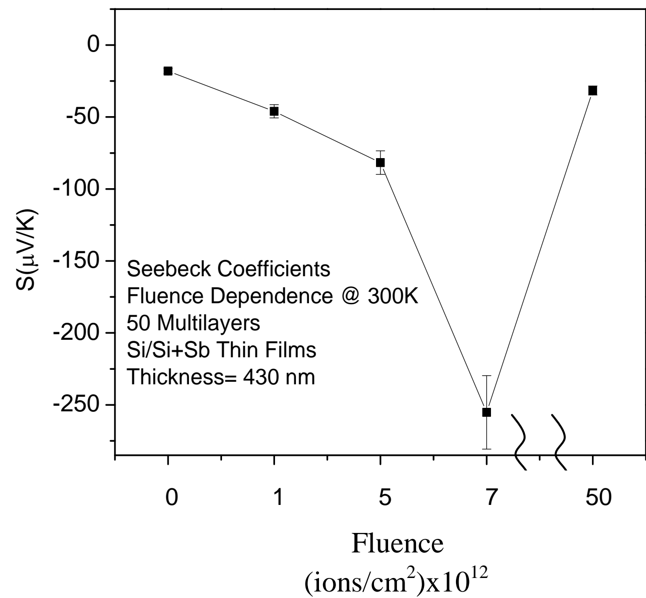

(b)

Figure 5.3 The fluence dependence of the cross-plane Seebeck coefficients of Si/Si+Sb multilayer thin films (a) at the different temperatures (b) at room temperature.

Ion bombardment of thin films causes disorder in the crystal structure of semiconductor thin films which decreases the electrical conductivity. However, an additional consequence is an increase in the density of electron states due to the structure formed by ion bombardment. Thus, cross-plane conductivity of the thin film actually increases. As a result of the enhanced density of electronic states, the cross-plane Seebeck coefficient of the ion bombarded thin film also increases. That is, the thermoelectric figure of merit of the film increases [16], [22].

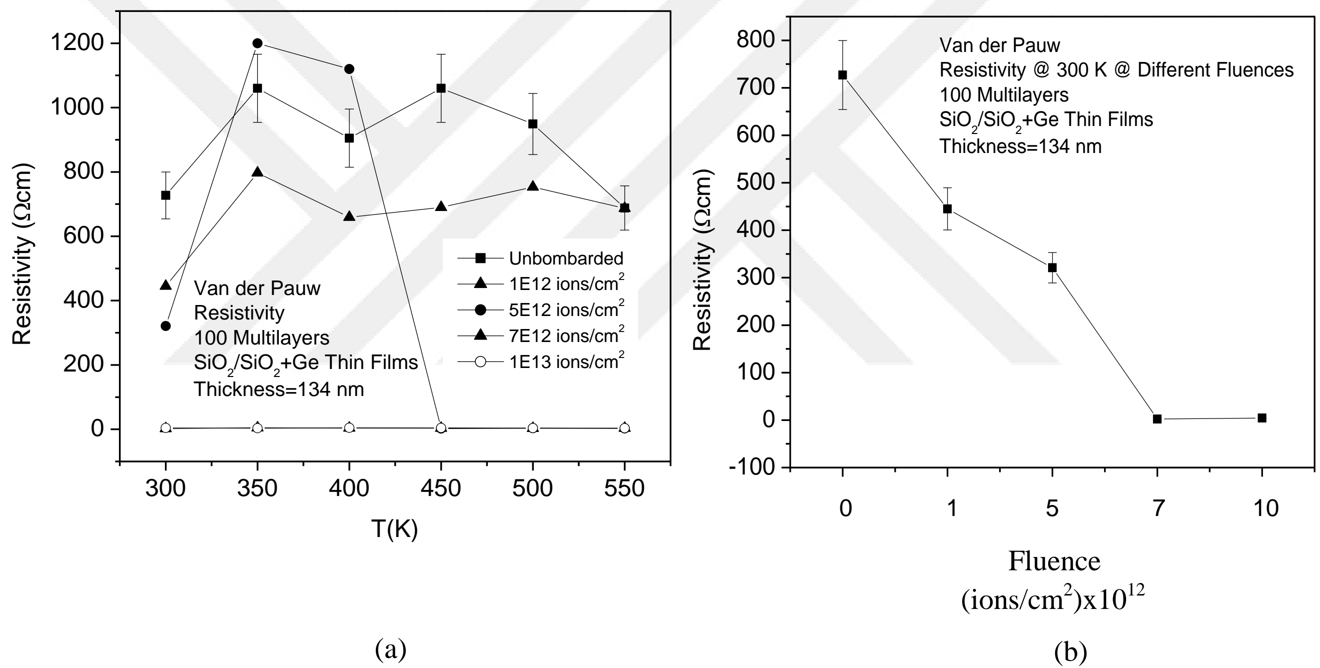

(a) (b)

Figure 5.4 The fluence dependence of Van der Pauw resistivity measurements of SiO_2/SiO_2+Ge multilayer thin films (a) at the various temperatures (b) at 300 K.

The Van der Pauw technique (see Appendix C) is a widely used technique that determining the resistivity of semiconductor samples. Measurement are taken by using four very small ohmic contacts which are in contact with the thin film plate, preferably in the corners.

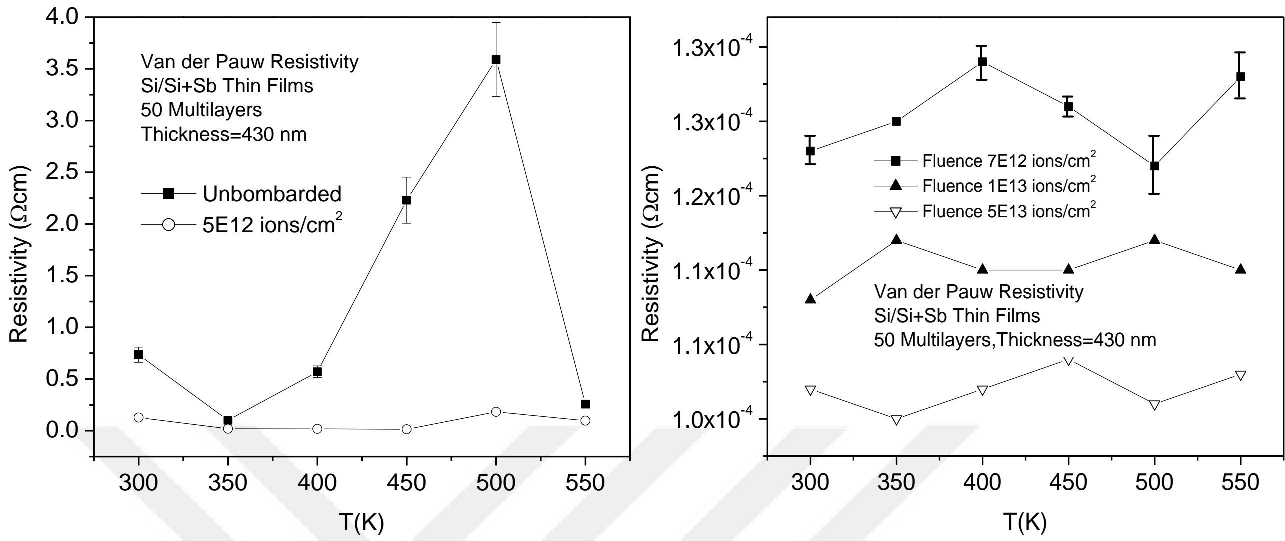

Figure 5.5 The fluence dependence of Van der Pauw resistivity measurements of Si/Si+Sb multilayer thin films at various annealing temperatures.

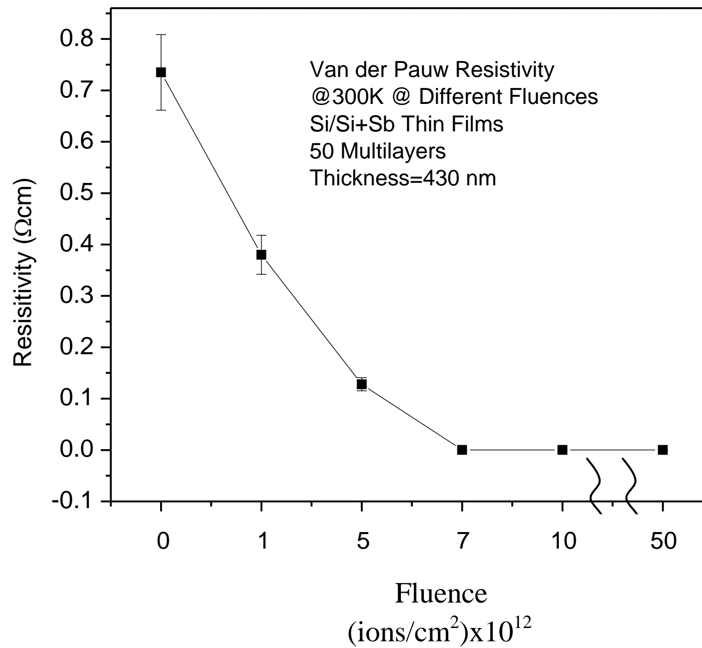

Figure 5.6 The fluence dependence of Van der Pauw resistivity measurements of Si/Si+Sb multilayer thin films at 300 K.

Figure 5.4 and 5.5 demonstrate the fluence dependences of the Van der Pauw resistivity of 100 alternating layers of SiO_2/SiO_2+Ge and 50 alternating layers of Si/Si+Sb thin films at temperatures between 300 K and 550 K respectively. The thin films were annealed for an hour over the temperature range 300 K to 550 K. There are increases and decreases in the resistivity values as seen in Figures 5.4 (a) and 5.5. The increases might be the result of annealing. However, Figures 5.4 (b) and 5.6 show that the resistivity values gradually decrease at 300 K with increasing bombardment fluence. This result is an expected behavior of semiconductor films exposed to ion bombardment. In Figure 5.4 (a) the data points for $7x10^{12}$ (triangle) ions/cm^2 and $1x10^{13}$ (circle) ions/cm^2 overlap. The result of the high energy Si ion bombardment is nano dots and/or nano clusters in the thin film structure. These formations are likely to be the reason for the increase in the number of majority charge carriers. During bombardment, electrons may gain enough energy to transition from the top of the valence band to the lowest part of the conduction band. In other words, the ion bombardment tends to lessen the gap between the valence band and conduction band. This causes a reduction in electrical resistivity and an increase in electrical conductivity. Creating this has been one of the goals in producing efficient thermoelectric devices [23].

Raman Spectroscopy analyzes the vibrational modes in a system, where laser light interacts with molecular vibrations or phonons, causing an energy shift [60]. The type and strength of the intermolecular interactions plays a crucial role in determining the resulting order of the molecules. Different molecular interactions are dominant depending on this order (H bonding or electrostatic forces) [68].

The phonon structure of the sample can be studied with Raman scattering, a technique well suited for the analysis of thin Ge films on Si [70]. A Dilor-JOBIN YVON-SPEX Raman Spectrometer was used to examine the SiO_2/SiO_2+Ge multilayer thin films for system order and bonds among the mentioned elements. The Raman spectra of SiO_2/SiO_2+Ge covers three broad regions corresponding to the modes of the Ge±Ge, Si±Si, and Si±O_2 bonds, respectively [69].

Figure 5.7 displays the temperature annealing dependence of the Raman Spectra of 100 multilayers of SiO_2/SiO_2+Ge thin films at different temperatures. Nine samples were used to obtain the Raman Spectra, and the samples were identical. Each sample was subjected to one specific annealing temperature. Figure 5.8 demonstrates the annealing temperature dependence of the Raman spectra for 100 multilayer SiO_2/SiO_2+Ge thin films. The peaks are attributed to a Ge-Ge mechanism in the polycrystalline layers at near 300 nm as shown in Figure 5.7 and in detail in Figure 5.8 (a). There is a peak in Figure 5.7 and 5.8 (b) around 525 nm corresponding to the single crystal Si substrate., However, the Ge contribution decreases, indicating that the amount of Ge in the thin film depends on the annealing temperature [21].

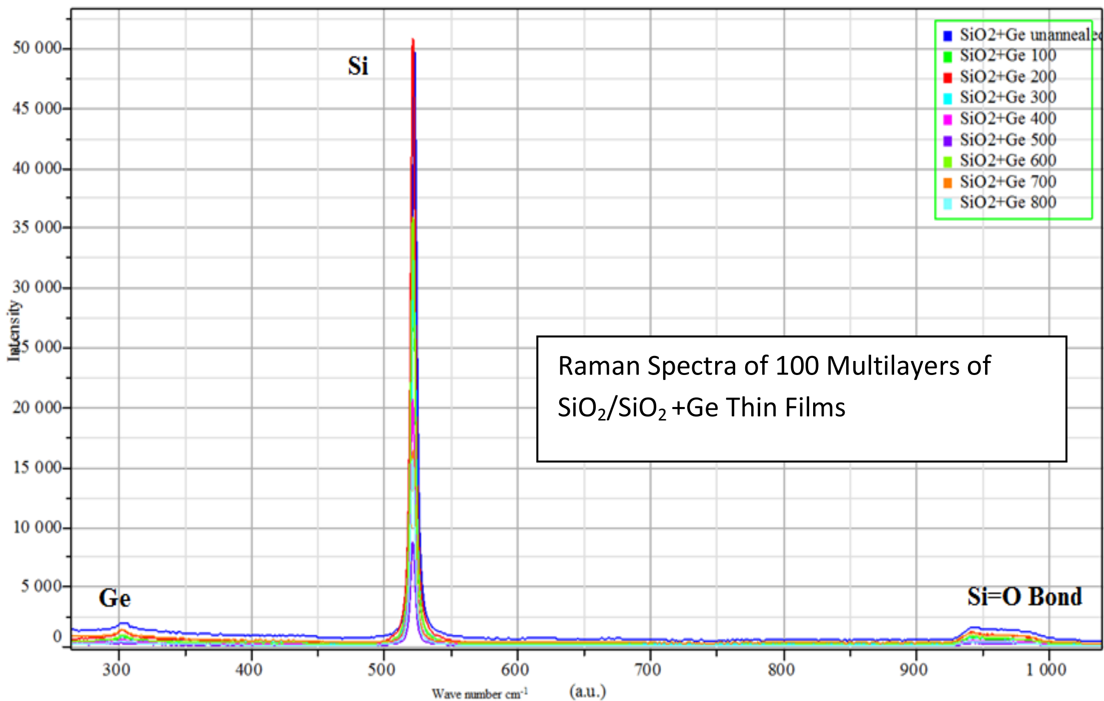

Figure 5.7 Raman Spectra of the thin films with 100 multilayers of SiO_2/SiO_2+Ge.

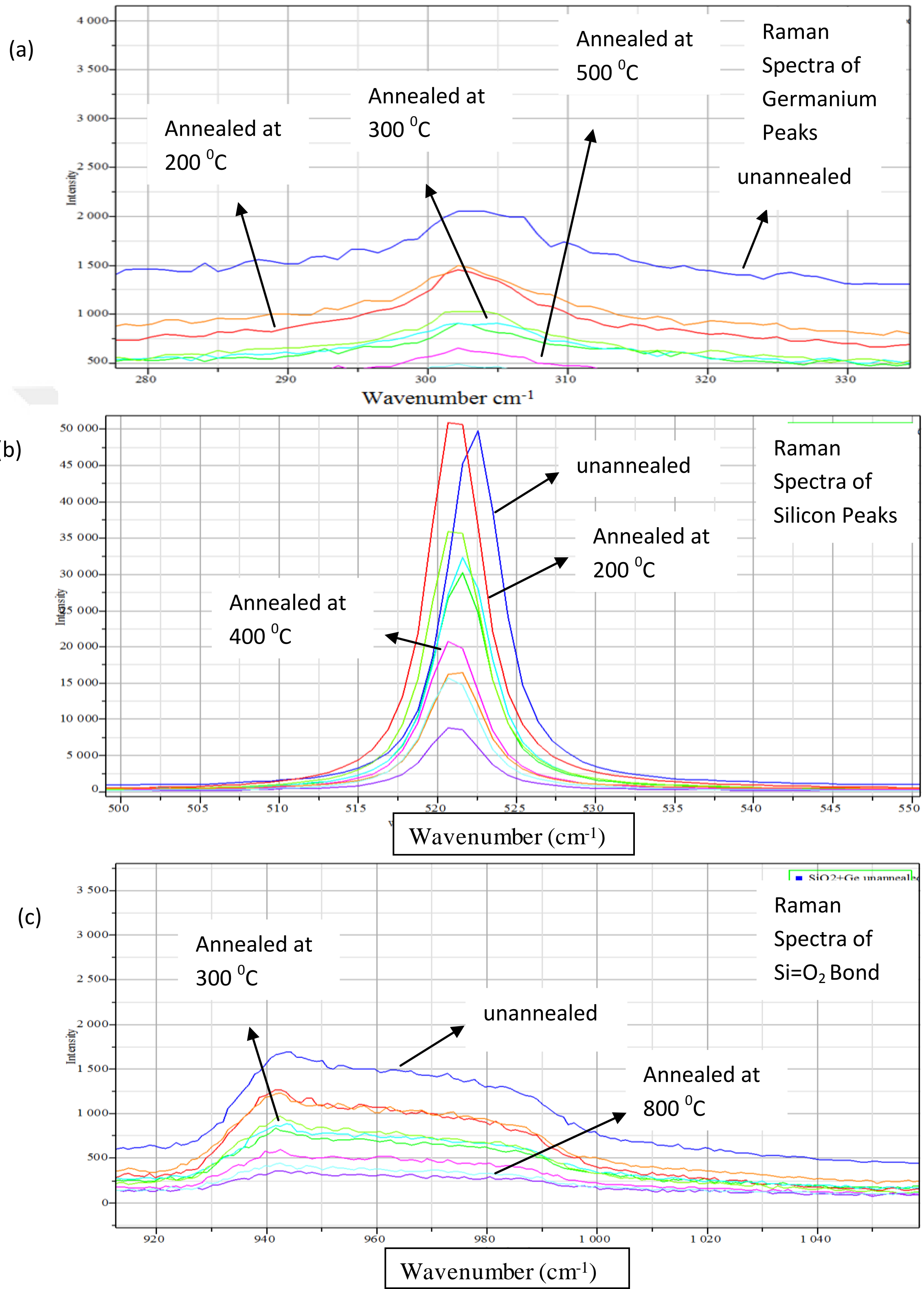

Figure 5.8 (a) Details of Raman Spectra of Ge peaks (b) Raman Spectra of Si peaks (c) Raman spectra of $Si{=}O_2$ bonds.

In Figure 5.9 (a), Raman Spectra of Si/Si+Sb thin films are shown at different fluencies for amorphous multilayer films. To be able to examine the multilayer films for order among the bonds of the mentioned elements, a Dilor-JOBIN YVON-SPEX Raman Spectrometer was used. Sb-Sb phonons are clearly distinguished in the energy-loss spectrum. The Sb-Sb phonons are especially important because they define the degree of intermixing across the Si-Sb interface. A peak at 200 nm suggests a Sb-Sb contribution from polycrystalline layers. A sharp high intensity peak is however observed around 160 nm, suggesting a single crystal contribution from the uannealed Sb substrate. Only a slight shift to 155 nm is seen after annealing at 100 ^{0}C as shown in Figure 5.9 (b) [61].

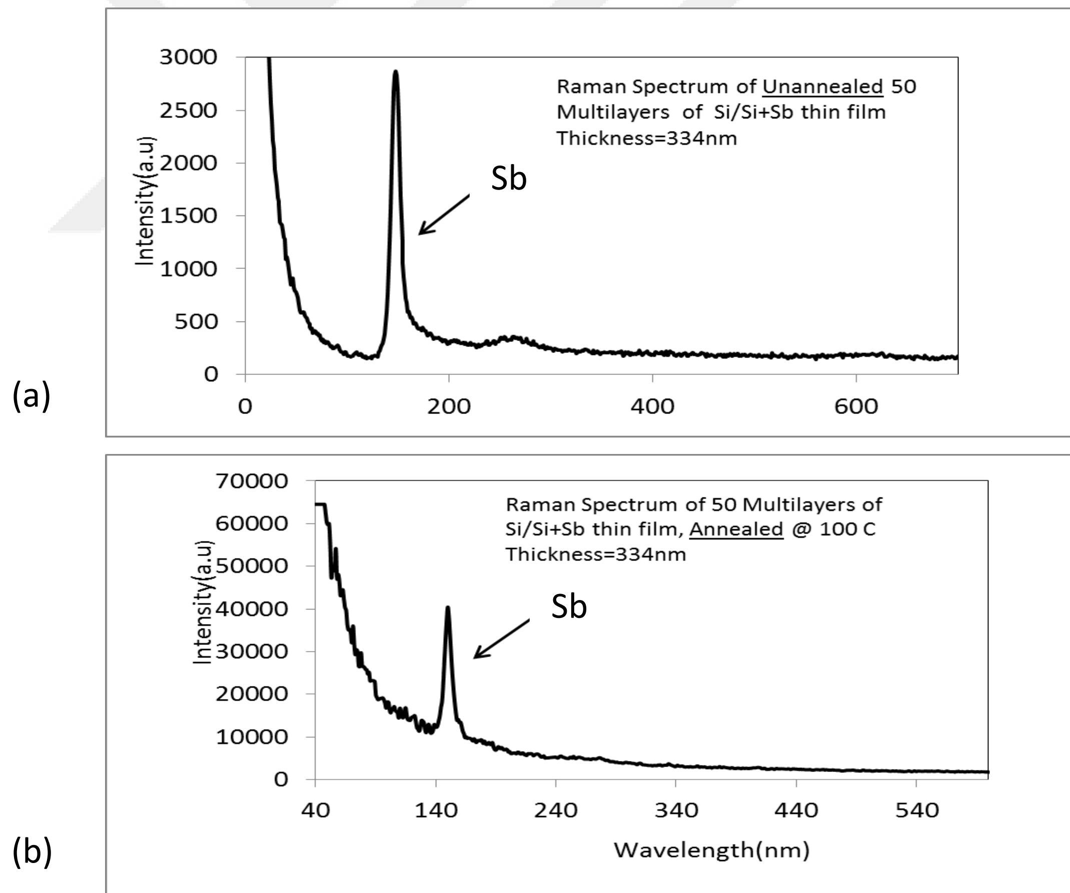

Figure 5.9 (a) Raman Spectrum of unnanealed 50 multilayers of Si/Si+Sb thin films, (b) Raman Spectrum of 50 multilayers of Si/Si+Sb thin films annealed at 100 ^{0}C.

Surface morphology of the Si/Si+Ge thin films is determined using the AFM technique.

Thickness, grain size, average roughness and rms roughness are crucial parameters for analyzing thin film microstructural properties. In this research, Si/Si+Ge thin films were deposited with thicknesses ranging from 5 to 25 nm onto n-type Si (100) substrates by ion beam deposition and were annealed for an hour at 100 ^{o}C and 200 ^{o}C so as to synthesize these multilayers.

The goal was to investigate the effects of annealing as a function of Si/Si+Ge thin film thickness. Grain size, grain height, and thus, surface roughness and film density increase with increased annealing time [26]. With increased annealing temperatures, an enhancement in the crystallinity of the film and crystallite sizes expected [25]. The observation is that there is a clear difference in the samples annealed for an hour at 200 ^{0}C (see Figure 5.12) with respect to surface roughness, shown in Fig. 5.11 and 5.12. In Figure 5.11 the 3D clusters are found to have lateral dimensions of 0–1000 nm and heights of 0–6 nm. However, in Figure 5.12 the lateral dimensions are between 0-5µm with heights between 0-25 nm. The films annealed at 100 ^{0}C are comparatively smoother [64].

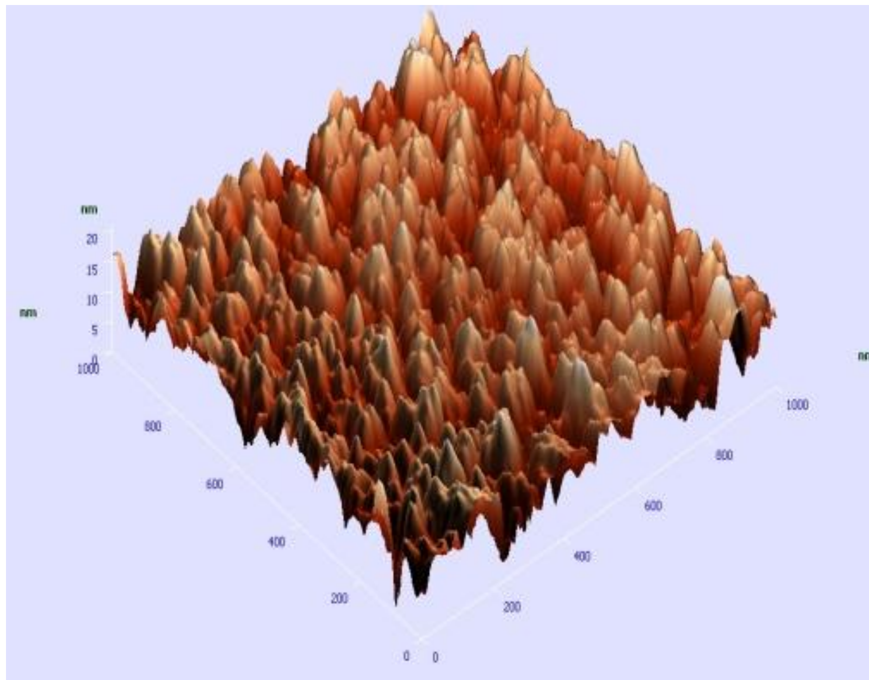

Figure 5.10 Atomic Force Microscopy (AFM) surface morphology of unannealed 40 multilayers of Si/Si+Ge thin film.

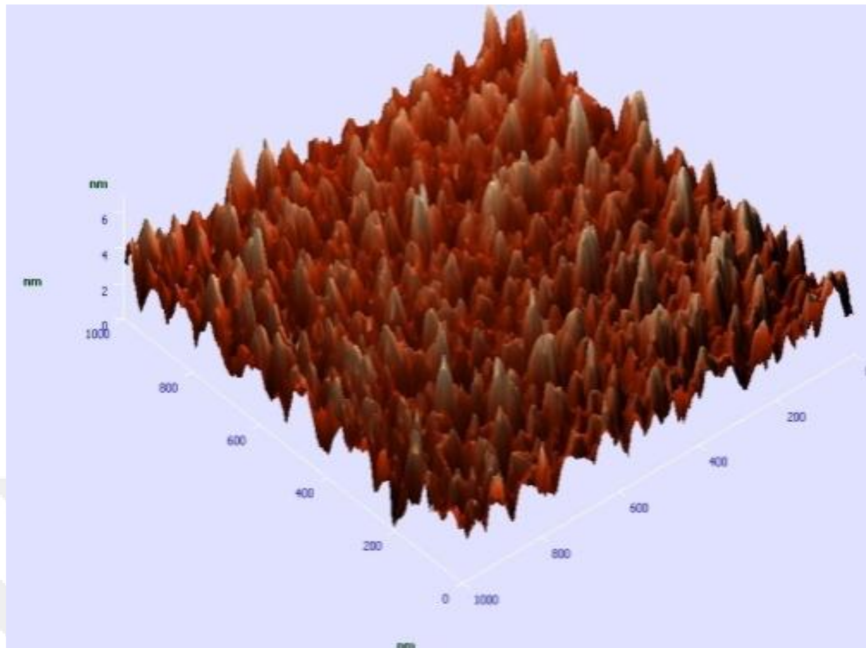

Figure 5.11 Atomic Force Microscopy (AFM) surface morphology of 40 multilayers of Si/Si+Ge thin films annealed at 100°C.

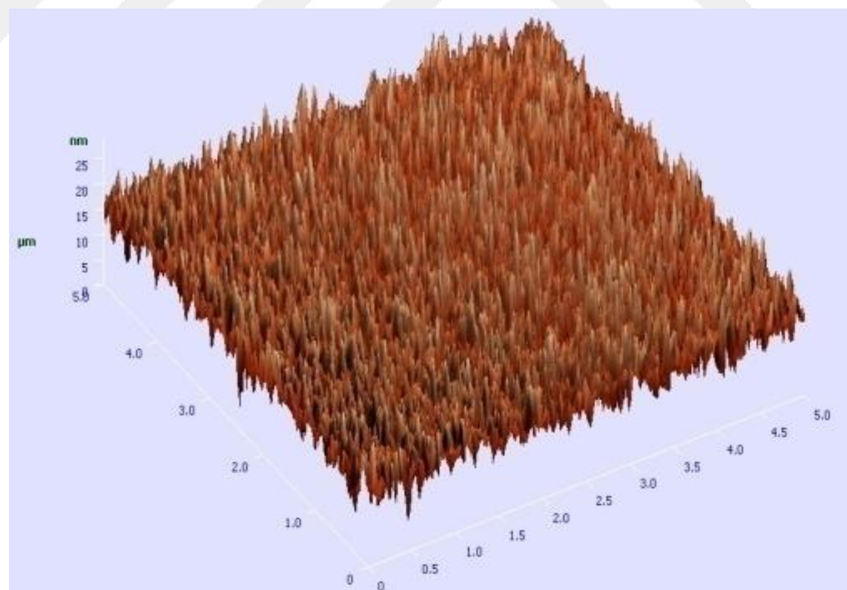

Figure 5.12 Atomic Force Microscopy (AFM) surface morphology of 40 multilayers of Si/Si+Ge thin films annealed at 200°C.

Antimony is in the nitrogen group (group 15) and has an electro negativity of 2.05. As expected from periodic table trends, it is more electronegative than tin or bismuth, and less

electronegative than tellurium or arsenic [11]. Antimony is increasingly being used more often in the semiconductor industry as a dopant for heavily doped n-type silicon wafers in the production of diodes [12], infrared detectors, and Hall-effect devices. In the 1950s, tiny beads of lead-antimony alloy were used to dope the emitters and collectors of n-p-n alloy junction transistors with antimony [13]. Indium antimonide is used as a material for mid-infrared detectors [14].

Since interest has increased in Si/Sb multilayer thin film technology, preparations of silicon (Si) doped with antimony (Sb) have motivated many studies in recent years. The surface morphology can be characterized by Atomic Force Microscopy (AFM). In Figure 5.13, and 5.15, the 3D clusters are found to have lateral dimensions of 0–1000 nm and heights of 0–12 nm. Figure 5.14 shows the lateral dimensions of 0–1000 nm and heights of 0–10 nm for Si/Si+Sb thin films annealed at 100 ^{0}C. Comparing these figures, the trend seems to be that as the annealing temperature increases, the surface become flatter and surface roughness increases. In addition the surface alternates clearly from irregularly rough to densely populated with dome-like structures [74].

The presence of Sb during the Si homo-epitaxy has dramatically altered the surface morphology. It is well known that Sb has a great effect on Si homo-epitaxy for nominal Si (111) surfaces [15]. Sb not only prevents the roughening of the surface, which occurs usually during the growth on disoriented substrates, but also flattens it (mono-atomic steps instead of tri-atomic ones). As a result of annealing, the surface of the Si/Si + Sb multilayer thin films became smoother, as shown in Figures 5.13, 5.14 and 5.15. If proper annealing temperatures can be determined, the efficiency of TE devices could be increased.

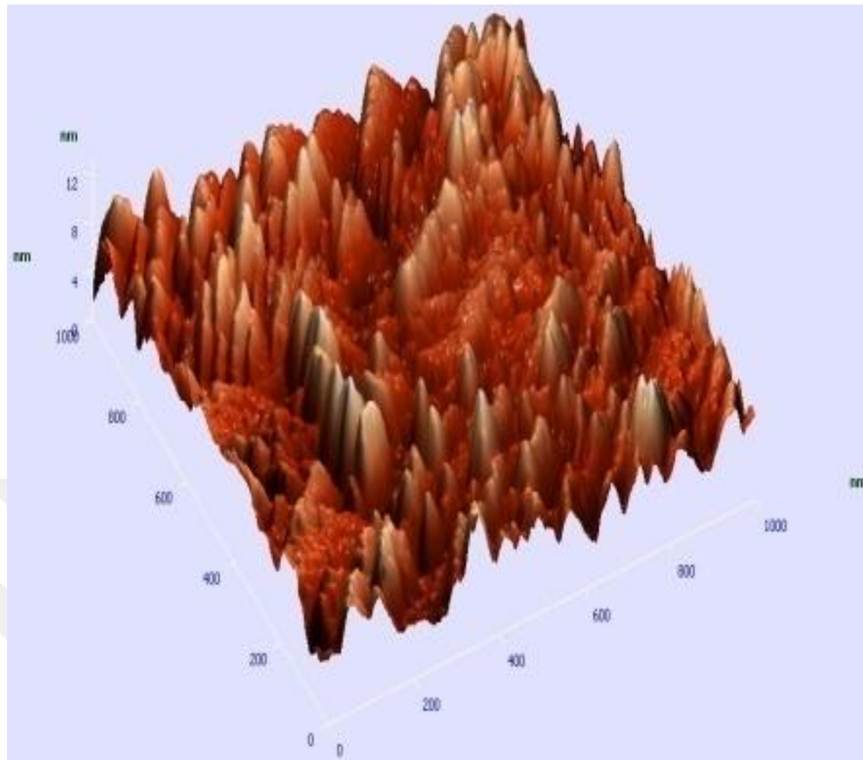

Figure 5.13 Atomic Force Microscopy (AFM) surface morphology of unannealed Si/Si+Sb thin films.

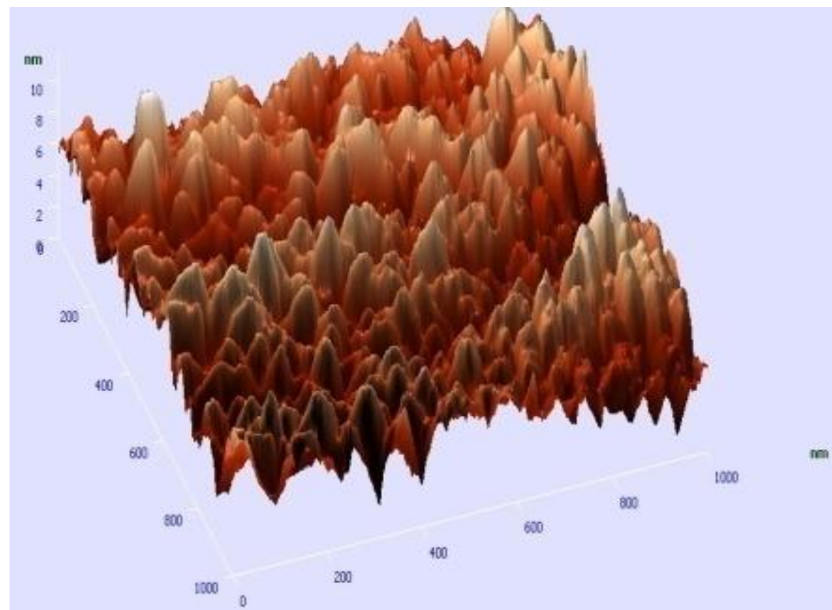

Figure 5.14 Atomic Force Microscopy (AFM) surface morphology of Si/Si+Sb thin films annealed at 100°C.

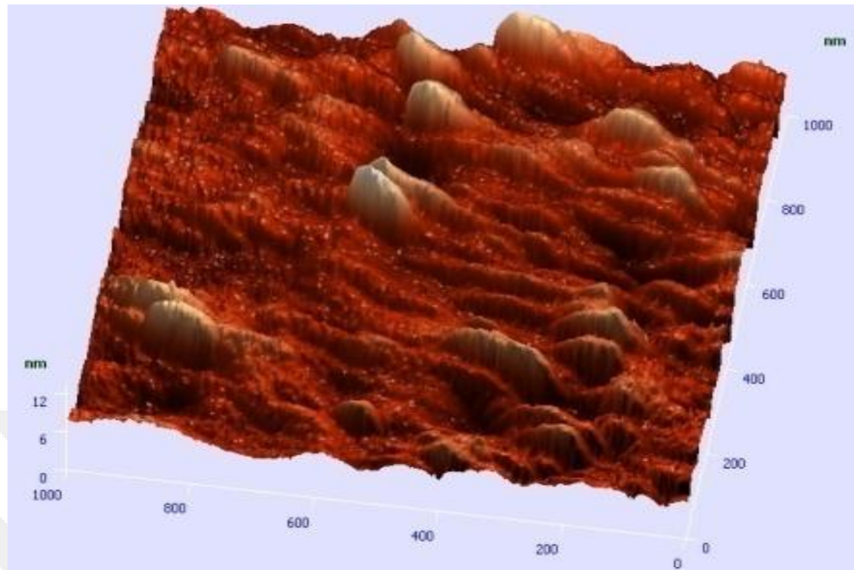

Figure 5.15 Atomic Force Microscopy (AFM) surface morphology of 50 multilayers of Si/Si+Sb thin films annealed at 200 ^{o}C.

To be able to measure the stoichiometry of each Si/Si+Ge and Si/Si+Sb layer identical multi-layer Si/Si+Ge and Si/Si+Sb superlattice thin films were grown on a glassy polymeric carbon (GPC) substrate for Rutherford backscattering spectroscopy (RBS) analysis. GPC was chosen for RBS measurements because carbon is a low mass substrate material that allows all possible elements used in the alternating layers to be detected, as seen in Figure 5.16 and Figure 5.17. RBS measurements were done using 2.1 MeV He+ ions. A silicion planar detector was located at 170° from the incident beam to monitor the thin film thickness and stoichiometry. Results are shown in Figures 5.16 and 5.17. Depending on the compostion of different layers, the thickness varied. Elements deposited on the substrates are detected at the energy channel numbers. Analyzed values of RBS were provided by a computer program called the Rutherford Universal Manipulation Program (RUMP).

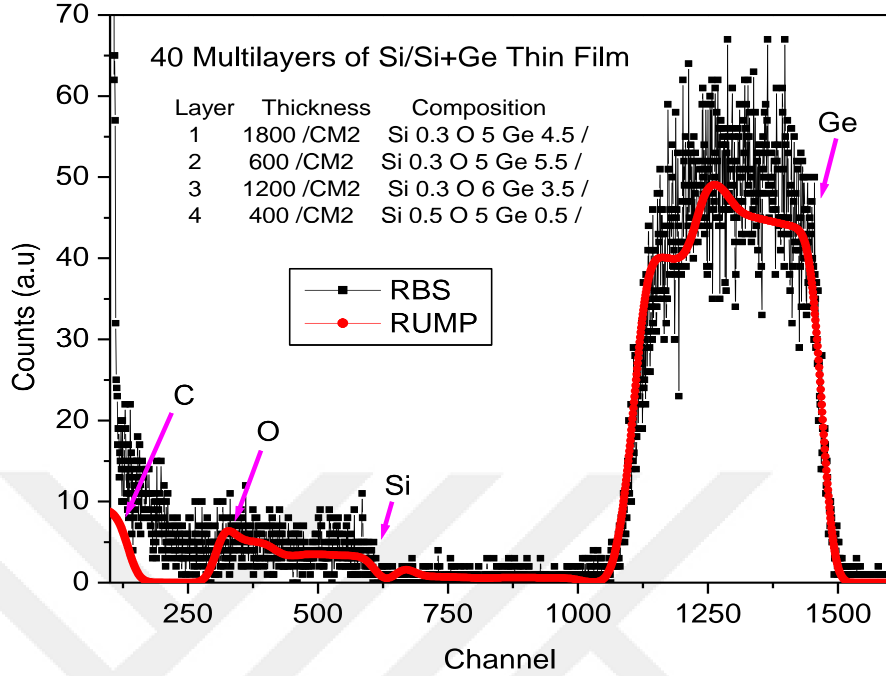

Figure 5.16 RBS and corresponding RUMP Simulation of Si/Si+Ge thin films.

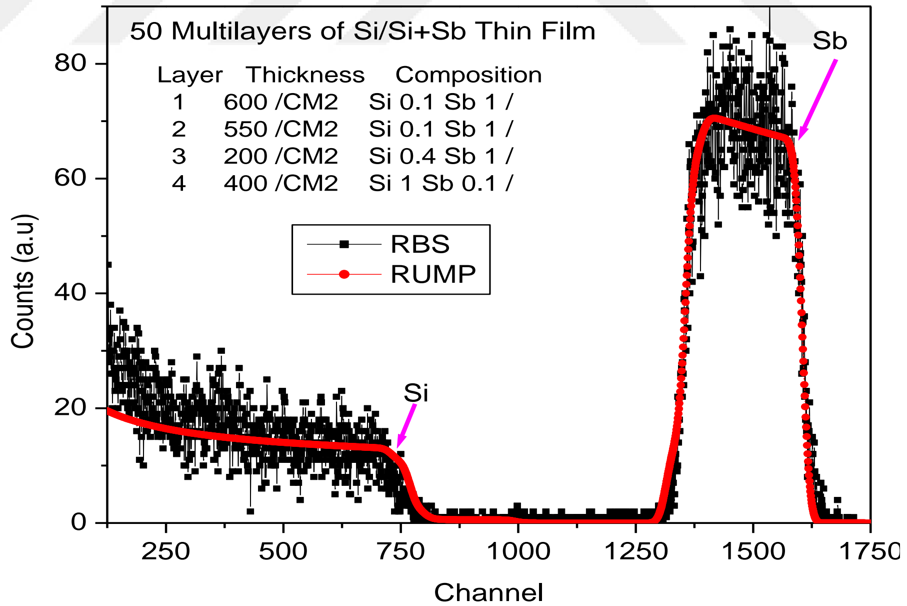

Figure 5.17 RBS and corresponding RUMP Simulation of Si/Si+Sb thin films.

V. CONCLUSION

One hundred alternating layers of SiO_2/SiO_2+Ge, 50 alternating layers of Si/Si+Sb, and 40 alternating layers of Si/Ge+Si nanolayers thin films have been deposited on silicon and silica (suprasil) substrates by using the technique of ion beam assisted deposition (IBAD) and DC/RF Sputtering. The Seebeck coefficients of SiO_2/SiO_2+Ge and Si/Si+Sb multilayer thin films have been characterized before and after MeV Si ion bombardment at five different fluencies. The Van der Pauw resistivities (see Appendix C) of SiO_2/SiO_2+Ge and Si/Si+Sb multilayer thin films have been investigated at different temperatures. Raman spectra of SiO_2/SiO_2+Ge and Si/Si+Sb multilayer thin films have also been studied. Raman measurements were made to gain information about order and bond formations in the multilayered systems. AFM images have been obtained for the Si/Si+Ge and Si/Si+Sb multilayer thin films in order to examine surface morphologies before and after annealing. In order to investigate the stoichiometry of each Si/Ge, and Si/Sb superlattice thin film layer, RBS data was taken and RUMP simulations were done. Because thermoelectric devices have a promising future as alternative energy sources, analyzing semiconductor thin film devices will continue in order to find higher efficiencies.

Thermoelectric (TE) modules have been used to convert waste heat to electricity and in cooling systems. Thermoelectric coolers and generators have a lot to offer regarding their advantages over traditional equipment because they are compact, reliable, quiet (no moving parts) and environmentally friendly. The automotive industry is interested in generating electrical power from waste engine heat. In addition, it is widely known that NASA's Voyager and Cassini missions used radioactive thermoelectric generators. A material's value for thermoelectric (TE) applications is indicated by the dimensionless figure of merit,

$$ZT = \frac{TS^2\sigma}{\kappa} \quad (5.1)\ [22]$$

where S is the Seebeck coefficient, σ is the electrical conductivity, T is the absolute temperature

in Kelvin, and κ is the thermal conductivity. An increase in the Seebeck coefficient S and a decrease in the thermal conductivity κ have been the goals in improving thermoelectric performance. Thin films have been used in this work because of the freedom to engineer the materials at nanoscales. Moreover, in this study, the data demonstrated that high energy ion bombardments and annealing can positively modify the thermoelectric properties of the multinanolayer superlattice thin films at specific fluencies and temperatures. In the future, research will likely continue on these materials to increase the figure of merit values [65], [66], [67].

APPENDIX A

Energy Band Theory

Energy bands occur in crystal structures, as shown in Figure A.1. Crystal structures can exist in almost all metals and semiconductors. In a crystal individual atoms form a very compact structure. Thus, the resulting energy levels are remade because of the interrelationship between the atoms. Unless the outer shell electrons, the energy levels of the inner shell electrons are not changed significantly when atoms fabricate crystals. Energy levels of the outer shell electrons can be modified noticeably since these electrons make bonds with the adjacent atoms in the crystalline structure [23].

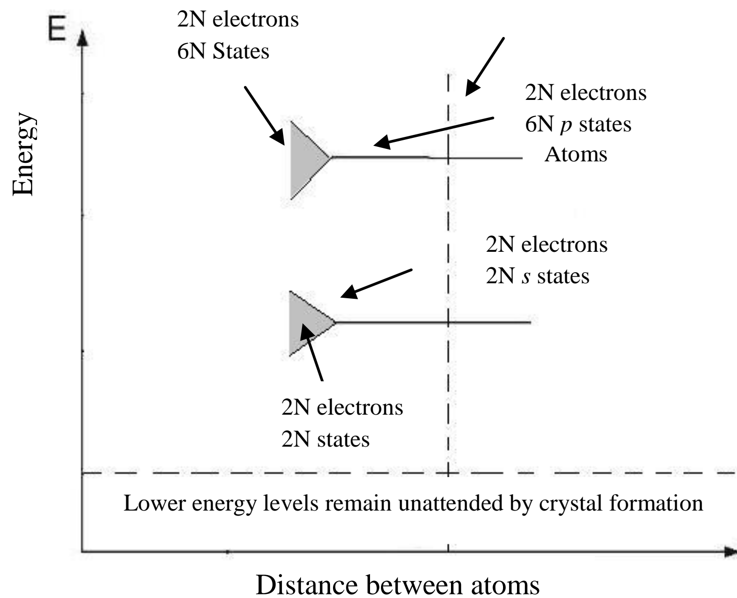

Figure A.1 Energy band formation in a crystal.

It is assumed that N silicon atoms form a crystal structure. The focus will be on the outermost electrons in silicon, because they will form bonds with the neighboring atoms. Silicon has 14 electrons in total, with electrons in the outermost orbits belonging to the 3s and 3p sub-shells, which contain 2N electrons. The distance between atoms will decrease as the interaction

becomes stronger between neighboring atoms, as shown in Figure A.1. Therefore, the wave functions of electrons in the outermost sub-shells will overlap. However, the lower energy levels will stay untouched in most cases [23].

APPENDIX B

Fermi Level

Figure B.1 displays the energy distribution of electrons in a metal. The Fermi level is defined as the energy level for which the probability of electron occupancy is 50% or 0.5 at any given time. All the states above the Fermi level are completely empty at 0 K, and all the states below the Fermi level are full. For temperatures of the system raises above 0 K, it will also raise the energy of some electrons will exceed the Fermi energy, and a different maximum energy value will be created. This E_{max} will rise only if there is a positive temperature rise in the system. In addition, increasing the temperature does not only raise the energy, but also states above the Fermi energy level will be filled by electrons to some extent. As a result of this, there will be vacancies available below the Fermi level for electrons [23], [27].

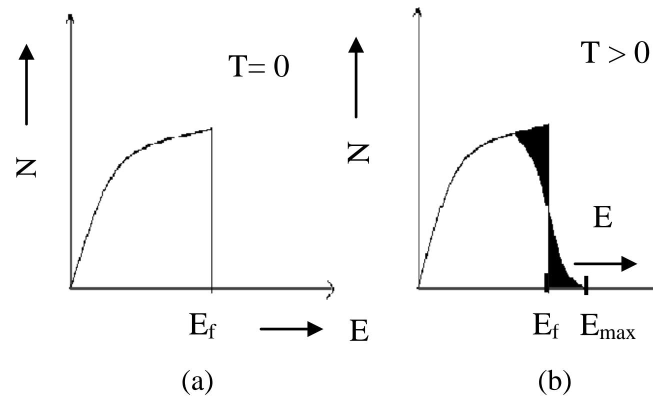

Figure B.1 Energy distribution of electrons in metals.

The probability F (E) of a state corresponding to energy E being occupied by an electron at temperature T (K) is given by

$$F(E) = \frac{1}{e^{\frac{E-E_f}{kT}}+1} \quad (B.1)$$

Here k is Boltzmann constant. Three cases of interest are:

(a) At T = 0 K, if $E > E_F$ then F (E) = 0, i.e., energy state is empty.

(b) At T = 0 K, if $E < E_F$ then F (E) = 1, i.e., energy state is occupied by an electron.

(c) At $T \neq 0$ K, and $E = E_F$ then F (E) = 1/2, i.e., energy state is 50% occupied.

Figure B.2 illustrates the position of the Fermi level in the energy band diagram. The Fermi level takes a position between the conduction and valence band, and does not depend on temperature. The Fermi level energy can be expressed as [23], [44];

Thus $$E_G = \frac{E_C + E_V}{2} \quad \text{(B.2)}$$ and

$$E_G = 2\,(E_F - E_V) \quad \text{(B.3)}$$

where E_G is the forbidden energy gap (≈ 1 eV)

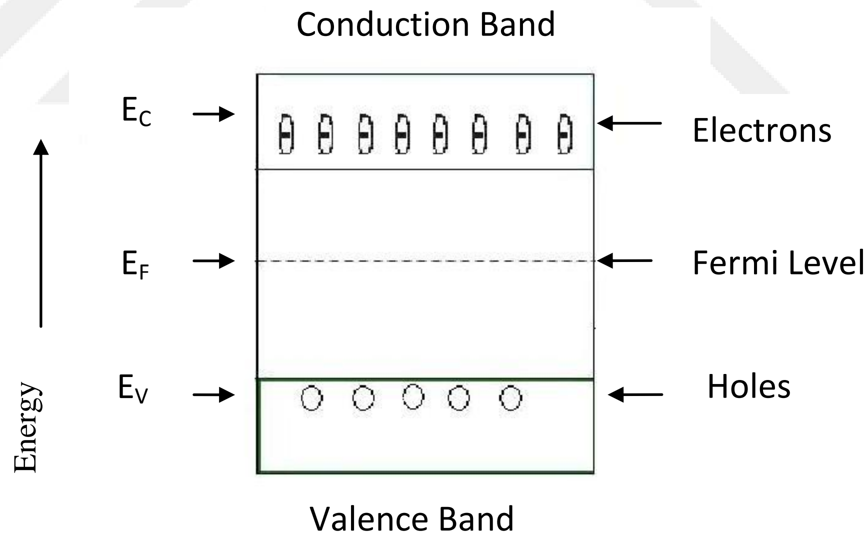

Figure B.2 Position of the Fermi level in energy band diagram at 0 K.

APPENDIX C

Van der Pauw Technique

A schematic of a rectangular Van der Pauw configuration is shown in Figure 2.2. Resistivity measurements determine the sheet resistance R_S. Depending on the terminal positions there are two characteristic resistances R_A and R_B, as shown in Figure C.1. The R_A and R_B are related to the sheet resistance R_S through the Van der Pauw equation [51]:

$$\exp(-\pi R_A/R_S) + \exp(-\pi R_B/R_S) = 1 \qquad (C.1)$$

Also the bulk electrical resistivity ρ can be calculated using:

$$\rho = R_S d. \qquad (C.2)$$

To obtain these two characteristic resistances, a DC current I is applied through contact 1 and out of the contact 2 and voltage measurements V_{43} are made from contact 4 to contact 3, as shown in Figure C.1 [51].

Next, current I is applied through contact 2 to contact 3 while measuring the voltage V_{14} from contact 1 to contact 4. R_A and R_B are calculated by means of the following expression [51]:

$$R_A = V_{43}/I_{12} \text{ and } R_B = V_{14}/I_{23} \qquad (C.3)$$

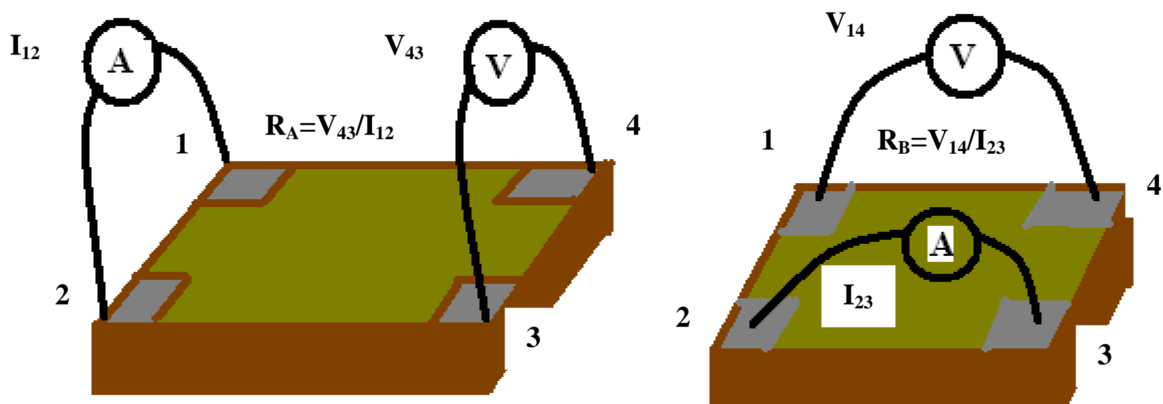

Figure C.1 Schematic of a Van der Pauw configuration used in the determination of the two characteristic resistances R_A and R_B.

REFERENCES

[1] Mildred S. Dresselhaus, Gang Chen, Ming Y. Tang, Ronggui Yang, Hohyun Lee, DezhiWang, ZhifengRen, Jean-Pierre Fleurial, and Pawan Gogna, “New Directions for Low-Dimensional Thermoelectric Materials”, Adv. Mater, 19, 1043 1053, 2007.

[2] Z.H. Dughaish, “Lead telluride as a thermoelectric material for thermoelectric power generation”, Physica B 322 205–223 (2002).

[3] Pierre F. P. Poudeu, Jonathan D. Angelo, Adam D. Downey, Jarrod L. Short, Timothy P. Hogan, and Mercouri G. Kanatzidis Angew, “High Thermoelectric Figure of Merit and Nanostructuring in Bulk p-type $Na_{1-x}Pb_mSb_yTe_{m+2}$”, Chem, 118, 3919 –3923, 2006.

[4] Francis J. DiSalvo, “Thermoelectric Cooling and Power Generation”, Science Vol 285, 30 July 1999.

[5] Moosa Hatami, Gerrit E. W. Bauer, Qinfang Zhang and Paul J. Kelly, “Thermoelectric effects in magnetic nanostructures”, Physical Review B 79, 174426, (2009).

[6] Luisa Consiglieri, “The Joule-Thomson effect on the thermoelectric conductors”, 35J55, 78A99, 80A20, MSC2000. Viewed Nov 4, 2013. http://ptmat.ptmat.fc.ul.pt/arquivo/docs/preprints/pdf/2007/lc-cmaf.pdf

[7] Chambers, R. G., “Thermoelectric effects and contact potentials”, Physics Education, 12(6), 374-380, (1977).

[8] Arman Molki, “Simple Demonstration of the Seebeck Effect”, Science Education Review, 9(3), 2010.

[9] Kuei Fang Hsu, Sim Loo, Fu Guo, Wei Chen, Jeffrey S. Dyck, CtiradUher, Tim Hogan, E. K. Polychroniadis, Mercouri G. Kanatzidis, “Cubic $AgPb_mSbTe_{2+m}$: Bulk Thermoelectric Materials with High Figure of Merit”, Vol 303 Science, 6 February 2004.

[10] Liang Zou, Bo-Ping Zhang, Zhen-Hua Ge, Chao Gao, Dai-Bing Zhang, and Yao-Chun Liu, “Size effect of SiO_2 on enhancing thermoelectric properties of $Cu_{1.8}S$”, Phys. Status Solidi A 210, No. 12, 2550–2555, DOI 10.1002/pssa.201330185 (2013).

[11] Wiberg, Egon; Wiberg, Nils and Holleman, Arnold Frederick, “*Inorganic Chemistry”*, Academic Press., ISBN 0-12-352651-5, (2001).

[12] O'Mara, William C.; Herring, Robert B.; Hunt, Lee Philip, *“Handbook of Semiconductor Silicon Technology”*. William Andrew, p. 473. ISBN 978-0-8155-1237-0(1990). .

[13] Maiti, C. K., “Selected Works of Professor Herbert Kroemer”, World Scientific, P., 101. ISBN 978-981-270-901-1, 2008.

[14] Kinch, Michael, *“Fundamentals of infrared detector materials”*, p. 35. ISBN 978-0-8194-6731-7, (2007).

[15] B. Voigtlander, A. Zinner, T. Weber and H. Bonzel, “Modification of growth kinetics in surfactant-mediated epitaxy”, Phys. Rev. B 51 7583, (1995).

[16] S. Budak, C.Smith, M.Pugh, K.Heidary, T.Colon, R.B.Johnson, C.Muntele, D.ila, “MeV Si ions bombardments effects on thermoelectric properties of SiO_2/SiO_2+Ge nanolayers”, Radiation Physics and Chemistry, 81 410–413, (2012).

[17] M. Mayer, “Materials Analysis Trieste”, LNS0822003 (2003). Viewed October 10, 2013. http://users.ictp.it/~pub_off/lectures/lns022/Mayer_1/Mayer_1.pdf

[18] Misni Misran, “Atomic Force Microscopy”, SCGS6314 (2007). Viewed September 18, 2013.
http://www.geocities.ws/misnimisran/AFM07lec.pdf

[19] Katrin Kneipp, Harald Kneipp, Irving Itzkan, Ramachandra R. Dasari, and Michael S. Feld, “Ultrasensitive chemical analysis by Raman spectroscopy”, Chem. Rev., 99, 2957-2975, 1999.

[20] M.S. Dresselhaus, G. Dresselhaus, R. Saito, A. Jorio, “Raman spectroscopy of carbon nanotubes”, Physics Reports 409 47–99, (2005).

[21] Lu P-X, Wu F, Han H-L, "Thermoelectric properties of rare earths filled CoSb3 based nanostructure skutterudite", Journal of Alloys and Compounds 505: 255–258, (2010).

[22] Satilmis Budak, Robert Parker, Cydale Smith, Claudiu Muntele, Kaveh Heidary, Ralph B Johnson and Daryush Ila, "Superlattice multinanolayered thin films of SiO_2/SiO_2 + Ge for thermoelectric device applications", Journal of Intelligent Material Systems and Structures DOI: 10.1177/1045389X13483022, (2013).

[23] Physical properties of Elements and Semiconductors, A Textbook of Electronics, Viewed June 3,2013.
http://www.newagepublishers.com/samplechapter/000011.pdf.

[24] Jeaneth Thokozile Kabini, "The Solid State interaction of Palladium with SiC", University of Pretoria, 2012. Viewed January 23, 2014.
http://upetd.up.ac.za/thesis/available/etd-05162013-161426/unrestricted/dissertation.pdf.

[25] Ying-Ge Yang, Hong-Lei Maa, Cheng-Shan Xueb, Hui-Zhao Zhuangb. Xiao-Tao Haoa, Jin Maa, Shu-Yun Teng, "Preparation and structural properties for GaN films grown on Si (1 1 1) by annealing", Applied Surface Science 193 254–260, (2002).

[26] Di Wu, Aidong Li, Huiqin Ling, Xiaobo Yin, Chuanzhen Ge, Mu Wang, Naiben Ming, "Preparation of $(Ba_{0.5}Sr_{0.5})TiO_3$ thin films by sol–gel method with rapid thermal annealing", Applied Surface Science 165 309–314, 2000.

[27] Fermi Level, Viewed October 17,2013.
http://hyperphysics.phy-astr.gsu.edu/hbase/solids/fermi.html#c1.

[28] David de Koninck, "Thermal Conductivity Measurements Using the 3-Omega Technique", McGill University, Montreal-Canada, 2008. Viewed June 5,2013.
http://www.physics.oregonstate.edu/~tate/TateLabWiki/lib/exe/fetch.php?media=thermal cond:thermal_conductivity_measurements_using_the_3-omega_technique_david_de_koninck_.pdf

[29] G. S. Nolas, T. J. R. Weakley, J. L. Cohn, R. Sharma, "Structural properties and thermal conductivity of crystalline Ge clathrates", Physical Review B Volume 61, Number 6, February 1, 2000-II.

[30] Terry M.Tritt and M.A. Subramanian, Guest Editors, MRS Bulletin, Volume 31, March 2006.

[31] Jyrki Tervo, Antti Manninen, RistoIlola, Hannu Hänninen, "State-of-the-art of Thermoelectric Materials Processing, Properties and Applications", VTT-WORK-124, 2009.

[32] Thermoelectric materials. Viewed February 7, 2014. http://en.wikipedia.org/wiki/Thermoelectric_materials.

[33] Ion Beam Assisted Deposition. Viewed December 13, 2013. http://www.spirecorp.com/spire-biomedical/surface-modification-technology/ion-beam-assisted-deposition.php.

[34] P.O. Offor, B.A. Ezekoye, "Fabrication of Annealing Furnace for Thin Film Characterizations, The Pacific Journal of Science and Technology", Volume 10, Number 2, November 2009.

[35] Semiconductor. Viewed February 22, 2013. https://eee.uci.edu/programs/hongchem/RDGsemiconductor.pdf.

[36] Band Theory of Semiconductors. Viewed January 18, 2013. http://chemwiki.ucdavis.edu/Physical_Chemistry/Quantum_Mechanics/Electronic_Structure/Band_Theory_of_Semiconductors

[37] Band Theory of Solids. Viewed July 12, 2013. http://hyperphysics.phy-astr.gsu.edu/hbase/solids/band.html.

[38] Insulator (electricity). Viewed May 19, 2013. http://en.wikipedia.org/wiki/Insulator_(electricity).

[39] Conductors and Insulators. Viewed May 5, 2013.

http://hyperphysics.phy-astr.gsu.edu/hbase/electric/conins.html.

[40] Charles Kittel, "*Introduction to Solid State Physics"*, 7th Ed., Wiley, 1996.

[41] The Doping of Semiconductors. Viewed May 16, 2013 http://hyperphysics.phy-astr.gsu.edu/hbase/solids/dope.html#c1.

[42] N –Type Semiconductor. Viewed June 5, 2013. http://simple.wikipedia.org/wiki/N-type_semiconductor.

[43] Extrinsic Semiconductor. Viewed May 9,2013. http://en.wikipedia.org/wiki/Extrinsic_semiconductor.

[44] E. Y. Tsymbal, Physics 927, Semiconductors. Viewed June 8, 2013. http://physics.unl.edu/tsymbal/teaching/SSP-927/Section%2012_Semiconductors.pdf.

[45] J.R. Hook, H.E. Hall, "*Solid State Physics* (2nd Edition)", Manchester Physics Series, John Wiley & Sons, ISBN 978-0-471-92804-1, 2010.

[46] Semiconductors and Band Theory. Viewed June 1, 2013. http://www.educationscotland.gov.uk/resources/nq/p/nqresource_tcm4658217.asp?strReferringChannel=educationscotland&strReferringPageID=tcm:4-615801-64.

[47] Senior Design Projects. Viewed May 8, 2013. http://www.ee.uconn.edu/SeniorDesign/projects/ecesd119/FinalReport.pdf.

[48] Novela Auparay, "Room Temperature Seebeck Coefficient Measurement of Metals and Semiconductors", Oregon State University, June 11, 2013. Viewed August 28, 2013. http://www.physics.oregonstate.edu/~tate/TateLabWiki/lib/exe/fetch.php?media=theses:auparay_bs_2013.pdf.

[49] Justin Kirschbrown, "RF/DC Magnetron Sputtering", November 20, 2007. Viewed November 23, 2013. http://www.unc.edu/~justink/RFDC_Sputtering.pdf.

[50] Temperature Dependence of Resistivity. Viewed June 11, 2013.

http://www.tutorvista.com/content/physics/physics-iv/current-electricity/temperature-resistivity.php.

[51] Maria P. Gutiérrez, Haiyong Li, and Jeffrey Patton, “Thin Film Surface Resistivity”, 2002. Viewed June 17, 2013. http://memd.cankaya.edu.tr/uploads/files/file/thin%20film%20surface%20resistivity.pdf.

[52] The Crystal Structure of Solids. Viewed May 25, 2013. http://highered.mcgraw-hill.com/sites/dl/free/0073529583/897250/Sample_Chapter.pdf.

[53] Extrinsic Semiconductors. Viewed June 19, 2013. http://chemwiki.ucdavis.edu/Physical_Chemistry/Quantum_Mechanics/Electronic_Structure/Extrinsic_Semiconductors.

[54] P-Type, N-Type Semiconductors. Viewed July 25, 2013. http://solarwiki.ucdavis.edu/The_Science_of_Solar/1._Basics/D._P-N_Junction_Diodes/I._P-Type,_N-Type_Semiconductors.

[55] T. B. Coplen, “Atomic Weights of the Elements 1999”, IUPAC, Pure & Appl. Chem., 73, 667, 2001.

[56] Atomic Spectroscopy, by W.C. Martin and W.L. Wiese in Atomic, Molecular, & Optical Physics Handbook, ed. by G.W.F. Drake (AIP, Woodbury, NY, 1996) Chapter 10, pp. 135–153O'Mara, William C.; Herring, Robert B.; Hunt, Lee Philip, Handbook of semiconductor silicon technology. William Andrew. p. 473. ISBN 978-0-8155-1237-0, (1990).

[57] Energy Levels. February 24, 2014. http://www.learner.org/interactives/periodic/elementary2.html.

[58] The Thermopile. Viewed November 2, 2013. http://scholar.lib.vt.edu/theses/available/etd-8497-205315/unrestricted/chap2.pdf.

[59] Gardiner, D.J., *“Practical Raman spectroscopy”*, Springer-Verlag, ISBN 978-0-387-50254-0 (1989).

[60] Olga Degtyareva, Viktor V. Struzhkin, and Russell J. Hemley, “High-pressure Raman spectroscopy of antimony: As-type, incommensurate host-guest, and bcc phases”, Solid State Communications 141 164–167, (2007).

[61] Satilmis Budak, Cydale Smith, Claudiu Muntele, Bopha Chhay, Kaveh Heidary, Ralph B Johnson and Daryush Ila, “Thermoelectric properties of SiO_2/SiO_2+CoSb multi-nanolayered thin films modified by MeV Si ions”, Journal of Intelligent Material Systems and Structures published online, DOI: 10.1177/1045389X12470302, 14 December 2012.

[62] P.K. Nair, M.T.S. Nair, V.M. Garcia, O.L. Arenas, Y. Pena, A. Castillo, I.T. Ayala, O. Gomezdaza, A. Sanchez, J. Campos, H. Hu, R. Suarez, M.E. Rincon, “Semiconductor thin films by chemical bath deposition for solar energy related applications”, Sol. Energy Mater. Sol. Cells 52 313-344, (1998).

[63] S.P. Nehra, M. Singh, “Effect of vacuum annealing and hydrogenation on ZnSe/Mn multilayer diluted magnetic semiconductor thin films”, Vacuum 85 719-724, (2011).

[64] Abdul Faheem Khan, Mazhar Mehmood, Anwar M. Rana, Taj Muhammad, “Effect of annealing on structural, optical and electrical properties of nanostructured Ge thin films”, Applied Surface Science 256 2031–2037, (2010).

[65] O. Yamashita, “Resultant Seebeck coefficient formulated by combining the Thomson effect with the intrinsic Seebeck coefficient of a thermoelectric element”, Energy Conversion and Management 50 2394–2399, (2009).

[66] K.-H. Wu, C.-I. Hung, “Effect of substrate on the spatial resolution of Seebeck coefficient measured on thermoelectric films”, International Journal of Thermal Sciences 49 2299-2308, (2010).

[67] *Encyclopedia of Materials*: Science and Technology

(ed.), Elsevier, Oxford, ISBN: 0-08-043152-6 pp. 1–11.

[68] S.Y. Mar, C. S. Chen, Y. S. Huang, K. K. Tiong, “Characterization of RuO_2 thin films by Raman spectroscopy”, Applied Surface Science 90 497-504, (1995).

[69] J. L. Gole, D.A. Dixon, “Transformation, Green to Orange-Red, of a Porous Silicon Photoluminescent Surface in Solution”, J. Phys. Chem. B 102, 33, 1998.

[70] M. Kammler, D. Reinking, K.R. Hofmann, M. Horn-von Hoegen, “Surfactant-mediated epitaxy of Ge on Si: progress in growth and electrical characterization”, Thin Solid Films 336 29-33, (1998).

[71] B. Zheng, Z. Xiao, B. Chhay, R. Zimmerman, D. Ila., “Improvement on thermoelectric properties of multilayered $Si_{1-x}Ge_x$/Si by ion beam bombardment”, Nucl. Instr. and Meth. in Phys. Res. B 266 73–78, (2008).

[72] A. Bouyard, X. Blanchet, D. Ila, C.I. Muntele, R.L. Zimmerman, “Application of MeV ion bombardment to create micro-scale annealing of Silica-Gold films”, Application of Accelerators in Research and Industry, AIP Conference Proceedings 680, p. 643, 2003.

[73] Theodorian Borca-Tasciuc, Weili Liu, Jianlin Liu, Taofang Zeng, David W. Song, “Thermal Conductivity of Si/Ge Superlattices”, 0-7803-5451-6/00/ IEEE (2000).

[74] I. Kovacevic, B. Pivac, P. Dubcek, H. Zorc, N. Radic, S. Bernstorff, M. Campione, A. Sassella, “Formation of Ge islands from a Ge layer on Si substrate during post-growth annealing”, Applied Surface Science 253 (2007) 3034–3040.

[75] Jan-Martin Wagner, Hilmar Straube, Otwin Breitenstein, Semiconductor Thermodynamics, Retreat 2009, Weimar, Viewed April 12, 2014. http://www1.mpi-halle.mpg.de/~jmwagner/Peltier_at_p-n_junction-corr.pdf